applied sciences

MDPI

Article

The Potential of Gas Switching Partial Oxidation Using Advanced Oxygen Carriers for Efficient H_2 Production with Inherent CO_2 Capture

Carlos Arnaiz del Pozo [1,*], Schalk Cloete [2], Ángel Jiménez Álvaro [1], Felix Donat [3] and Shahriar Amini [4]

[1] Departamento de Ingeniería Energética, Escuela Técnica Superior de Ingenieros Industriales (ETSII) c/ José Gutiérrez Abascal nº2, Universidad Politécnica de Madrid, 28006 Madrid, Spain; a.jimenez@upm.es
[2] Flow Technology Research Group, SINTEF Industry, 7465 Trondheim, Norway; schalk.cloete@sintef.no
[3] Department of Mechanical and Process Engineering, Institute of Energy and Process Engineering, Eidgenössische Technische Hochschule ETH Zurich, 8092 Zürich, Switzerland; donatf@ethz.ch
[4] Department of Mechanical Engineering, South Engineering Research Center, University of Alabama, Tuscaloosa, AL 35487, USA; samini3@ua.edu
* Correspondence: cr.arnaiz@upm.es

Abstract: The hydrogen economy has received resurging interest in recent years, as more countries commit to net-zero CO_2 emissions around the mid-century. "Blue" hydrogen from natural gas with CO_2 capture and storage (CCS) is one promising sustainable hydrogen supply option. Although conventional CO_2 capture imposes a large energy penalty, advanced process concepts using the chemical looping principle can produce blue hydrogen at efficiencies even exceeding the conventional steam methane reforming (SMR) process without CCS. One such configuration is gas switching reforming (GSR), which uses a Ni-based oxygen carrier material to catalyze the SMR reaction and efficiently supply the required process heat by combusting an off-gas fuel with integrated CO_2 capture. The present study investigates the potential of advanced La-Fe-based oxygen carrier materials to further increase this advantage using a gas switching partial oxidation (GSPOX) process. These materials can overcome the equilibrium limitations facing conventional catalytic SMR and achieve direct hydrogen production using a water-splitting reaction. Results showed that the GSPOX process can achieve mild efficiency improvements relative to GSR in the range of 0.6–4.1%-points, with the upper bound only achievable by large power and H_2 co-production plants employing a highly efficient power cycle. These performance gains and the avoidance of toxicity challenges posed by Ni-based oxygen carriers create a solid case for the further development of these advanced materials. If successful, results from this work indicate that GSPOX blue hydrogen plants can outperform an SMR benchmark with conventional CO_2 capture by more than 10%-points, both in terms of efficiency and CO_2 avoidance.

Keywords: H_2-power cogeneration; gas switching partial oxidation; gas switching reforming; CO_2 capture and storage; steam methane reforming; blue hydrogen

Citation: Arnaiz del Pozo, C.; Cloete, S.; Jiménez Álvaro, Á.; Donat, F.; Amini, S. The Potential of Gas Switching Partial Oxidation Using Advanced Oxygen Carriers for Efficient H_2 Production with Inherent CO_2 Capture. *Appl. Sci.* **2021**, *11*, 4713. https://doi.org/10.3390/app11104713

Academic Editor: Magnus Rydén

Received: 26 April 2021
Accepted: 17 May 2021
Published: 20 May 2021

1. Introduction

Due to the growing concern of global warming caused by greenhouse gases (GHG) as highlighted in the IPCC Special Report [1], large-scale hydrogen production processes avoiding carbonaceous emissions have received increased attention. H_2 has a great potential to become the most attractive energy vector for decarbonizing several industry sectors, long-distance transport and gas heating networks, as discussed in the recent IEA report [2]. A comprehensive summary of current H_2 generation sources with present and projected end use to the year 2050 is presented by Voldsund et al. [3]. A detailed review of the different technological pathways for H_2 production has been carried out by Nazir et al. [4], while a study of the different applications and challenges of H_2 for the decarbonization of industry and energy sectors is provided in Nazir et al. [5].

Using an excess of renewable energy to produce H_2 from water electrolysis ("green hydrogen") is a promising pathway avoiding CO_2 emissions, as suggested by Parra et al. [6]. Schnuelle et al. carried out a techno-economic assessment of an electrolyzer with direct renewable electricity supply achieving a minimum cost of 4.33 €/kg of H_2 when powered with the onshore wind [7]. However, 95% of the total H_2 produced is currently originated from fossil fuels and the traditional pathway through natural gas reforming with steam (SMR), is responsible for approximately 50% of the total H_2 production. Furthermore, it will remain more cost-effective when integrating CCS technologies ("blue hydrogen") in several world regions [2]. For example, natural gas exporting regions like Norway can achieve an approximately 1 €/kg lower-levelized cost of H_2 with CCS than electrolysis [8]. In addition, this comparison does not account for the cost of intermittent hydrogen production from electrolyzers powered by wind and solar power, which adds substantial further costs, increasing the gap between blue and green hydrogen even for natural gas importers like Germany, as assessed by Cloete et al. [9]. If significant fossil fuel-based electricity generation is still on the grid, certification of green hydrogen production can be challenging. Some studies indicate the low development prospects of green hydrogen in the short term [10]. Nonetheless, blue hydrogen faces a relatively high energy penalty compared to the unabated process that results in large CO_2 avoidance costs (100 €/ton), well above the actual emissions tax, as reported by Spallina et al. [11]. Cormos et al. revealed that SMR with shifted syngas CO_2 absorption is the most cost-effective pathway for CO_2 abatement in H_2 production processes from natural gas with currently deployable technology [12]. Pre-combustion capture costs can be potentially reduced as membrane technology advances (with simpler fabrication methods from cheaper raw materials yielding enhanced performances, as studied by Miricioiu et al. [13,14]) by simplifying the separation processes (PSA and MDEA unit). Alternatively, the use of cheap adsorbents from waste-derived materials can increase the competitiveness of post-combustion capture [15], avoiding costly absorption systems.

On the other hand, Chemical Looping Combustion (CLC) first proposed by Ishida et al. offers the possibility of avoiding this large energy penalty by combusting a carbonaceous fuel with inherent CO_2 capture [16]. This is achieved by splitting the combustion reaction into two steps. CLC exposes a metallic oxygen carrier to oxidizing (e.g., air) and reducing (e.g., natural gas) streams in two separate reactors to avoid the mixing of the combustion products (CO_2/H_2O) with N_2. The oxygen carrier is hydrodynamically transported from one reactor to another, typically operating under fluidization conditions for efficient heat transfer. Alternative to full combustion of natural gas, Chemical Looping Reforming (CLR), developed by Rydén et al., obtains an H_2-rich syngas stream in the reduction outlet [17]. Subsequent water gas shift and CO_2 removal with MDEA is still required, as modeled by Nazir et al. [18]. Membrane-assisted chemical looping reforming (MA-CLR) has been proposed by Spallina et al. as an effective way to practically eliminate the energy penalty of CO_2 capture [11], but still requires several more development steps to de-risk and commercialize the complex system consisting of a membrane operating in a fluidized environment. Furthermore, a critical factor that hinders chemical looping applications is the slow scale-up under pressurized conditions required for efficient integration in power and chemical processes [19].

To overcome this challenge and avoid the operational difficulty of solids transportation between reactors, the gas switching (GS) technology has been suggested as a promising solution by Zaabout et al. [20]. Syngas production through the gas switching concept was experimentally demonstrated by Wassie et al. [21]. The oxygen carrier remains in the same reactor vessel while it is exposed alternatively to reducing, oxidizing and reforming steps by switching the feed and product streams by means of high-temperature valve mechanism. Gas Switching Reforming (GSR) appears as a highly attractive technological candidate for a step-change in H_2 production with CCS as shown by Nazir et al. [22], in which the reforming (H_2 production) and reduction (heat supply) steps are intrinsically decoupled, allowing for effective integration with the pressure swing adsorption unit

(PSA), as suggested by Spallina et al. for packed bed dynamically operated reactors [23]. Very attractive prospects in terms of efficiency and emissions avoidance, with compelling economic assessment results carried out by Nazir et al. suggest that further research and development should be conducted [24].

The oxygen carrier is central to every chemical looping process, and its activity, selectivity and long-term stability are important to ensure high overall process efficiency. Many different types of oxygen carriers have been investigated experimentally for chemical looping reforming, most of them based on iron oxide. Zaabout et al. investigated iron oxide supported on gamma–alumina particles and found that the addition of nickel was beneficial to achieve a higher conversion of the methane (which was used as a surrogate for natural gas) than pure iron oxide at 800 °C [25,26]. Similar observations were made by Kang et al. when adding small amounts (~1 wt.%) of nickel or yttrium to the oxygen carrier [27,28]. In contrast, the partial substitution of iron oxide with ceria did not improve the performance significantly [26]. Other oxygen carrier compositions have been reviewed recently [29,30], and from these studies, it is apparent that mixed oxides composed of several redox-active oxides can have synergistic effects with regard to their activity and syngas selectivity. An important problem to overcome in the chemical looping-based reforming scheme is the deposition of carbon on the surface of the oxygen carrier due to the cracking reaction of methane that is catalyzed by metallic iron. Carbon deposits could potentially be combusted in the oxidation step of the process (see below) and therefore lower the CO_2 capture efficiency. Perovskite-based oxygen carriers (e.g., $LaFeO_3$ with various dopants partially substituting the cations La and Fe) have shown promise in reducing carbon deposition while possessing a high selectivity towards syngas and a high reactivity due to their high oxygen mobility [30]. Our recent experimental studies have demonstrated that some perovskite-based oxygen carrier formulations (e.g., $La_{0.85}Sr_{0.15}FeO_3$ or $La_{0.85}Sr_{0.15}Fe_{0.95}Al_{0.05}O_3$) possess excellent long-term stabilities in reactor systems of different scales.

With the purpose of delving further into the potential of gas switching chemical looping integration for H_2 production, this study aims to evaluate one of these experimentally proven oxygen carriers in an integrated plant model. Instead of requiring a catalytically-active component (e.g., Nickel), this material possesses thermodynamic properties that enable the partial oxidation of methane (or natural gas) to syngas at near 100% selectivity, as reported by Donat et al. [31].

The Gas Switching Partial Oxidation (GSPOX) Process Concept

Relative to the GSR process, GSPOX enables the reforming step to be split into separate partial oxidation and water splitting steps. In addition, the Lanthanum-based oxidation carrier presents the opportunity to overcome the equilibrium limitations faced by catalytic natural gas reforming at higher pressures. The process configurations presented in this study aim to quantify the potential efficiency benefits of these oxygen carrier features.

Figure 1 shows the 3-step GSR operation and the two four-step GSPOX operating modes investigated. The first GSPOX configuration is designed to produce an H_2-rich syngas with minimal steam addition for maximum H_2 production efficiencies. In this case, the key GSPOX benefit is avoidance of equilibrium limitations in the reforming step, eliminating the need for high S/C ratios to achieve sufficient methane conversion at elevated pressures. The second GSPOX configuration targets combined H_2 and power production. In this case, the reforming step is split into partial oxidation and water splitting steps and the H_2 from the water-splitting step is used for low-carbon power production.

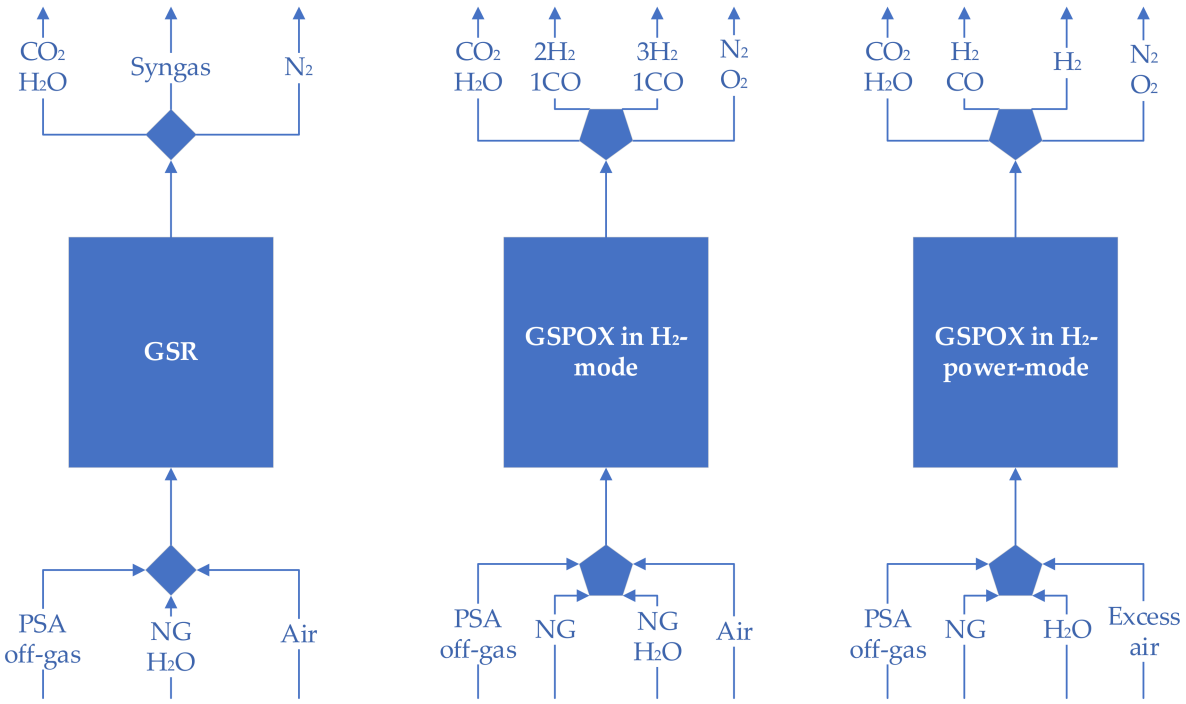

Figure 1. Illustration of the different reactor steps in the two GS reactor concepts.

For the GSPOX H_2-mode simulations, the process flowsheet is similar to previous GSR studies [22]. A schematic of the GSPOX H_2-power concept is presented in Figure 2 The water-splitting step in the GSPOX process produces an H_2 stream with some N_2 and CO from undesired mixing between the different reactor steps. This stream does not meet H_2 export purity requirements, but it is well-suited for combustion with the hot depleted air stream from the oxidation step for highly efficient low-carbon power production. Meanwhile, the 2:1 H_2:CO stream from the partial oxidation step is sent to a PSA unit for separating out ultra-pure H_2 for export. The remaining PSA off-gas stream is sent to the reduction step where it is oxidized to yield a high-purity CO_2 stream after water condensation. This PSA off-gas stream contains enough heating value to supply heat for the endothermic reforming reaction and the pre-heating of surplus air in the oxidation step for power production.

Relative to the previous GSR studies, the GSPOX concept developed in this study aims to evaluate:

- An alternative oxygen carrier for H_2 production plants with comparable efficiency levels, mitigating the safety concerns related to Nickel. Furthermore, the influence of operating pressure on the performance of GSR and GSPOX designs is assessed.
- A process design that eliminates the potentially disadvantageous feature of electricity consumption in H_2 production plants with CCS, by efficiently integrating a power cycle with the cluster, making effective use of the low-grade heat sources throughout the plant for additional electricity production, instead of LP steam export. The GSPOX concepts present a significant electricity output as an additional revenue source.
- A simplification of the plant section dedicated to H_2 production, by eliminating the water gas shift conversion and associated heat recovery units, substantially reducing the Steam to Carbon (S/C) plant requirements for natural gas conversion, and therefore reducing capital costs.
- From a modeling perspective, this study provides an integrated plant model between the dynamic clusters (GSR and GSPOX) and the stationary flowsheet simulation, avoiding cumbersome information exchange interfaces between platforms, making the process synthesis and evaluation more agile.

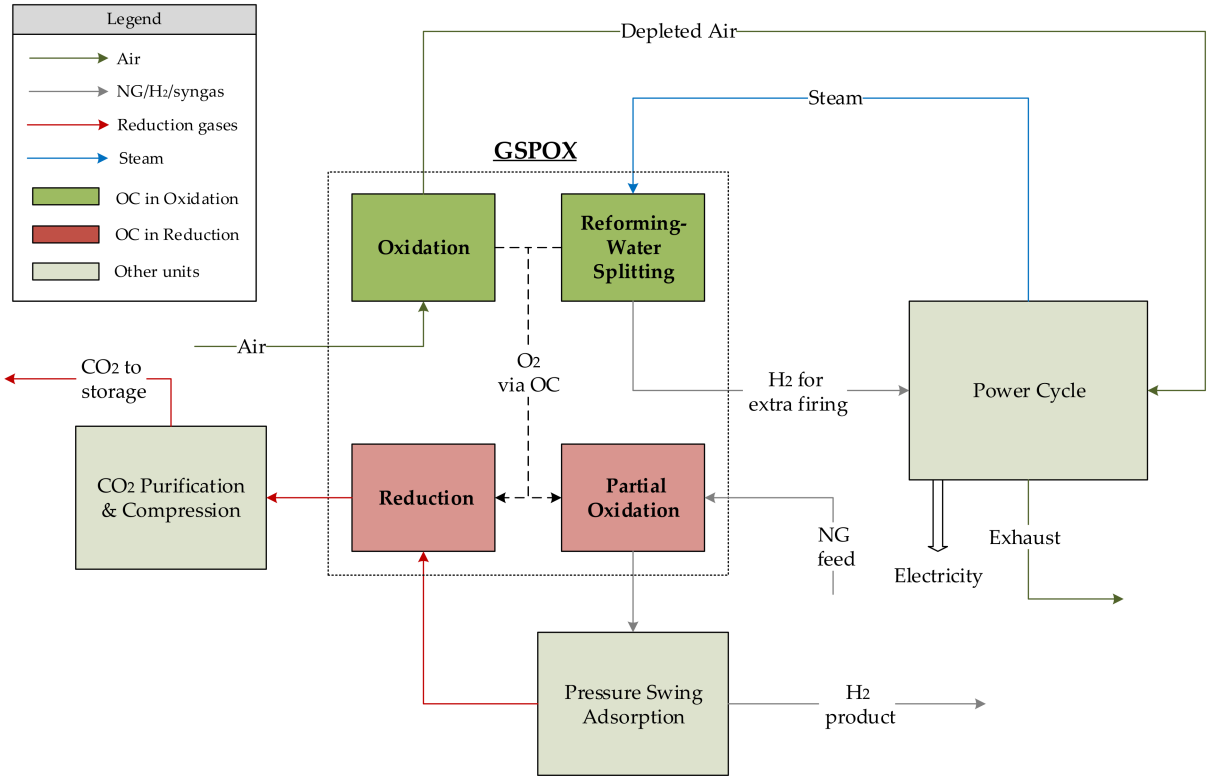

Figure 2. Simplified process diagram of the GPOX H_2-power plant.

This new process topology will be benchmarked against conventional unabated SMR plant, SMR with MDEA CO_2 capture and the previously studied GSR-H_2 plant, under consistent modeling assumptions. The following section provides a detailed description of the dynamic model development and its integration in the process flowsheet. The narrative for the GS-based H_2 and electricity production plants as well as the different benchmark processes is provided. Subsequently, the key performance indicators of the plants are presented based on pre-defined reference technologies, and a brief description of the modeling approach for the essential technological components is given. Results are shown attending to the efficiency definitions, energy breakdown across the plant and CO_2 emissions performance. Finally, the key results are summarized, and the main conclusions of this study are discussed.

2. Methodology

In this section, the modeling procedure and main assumptions taken for the representation of the transient GSR and GSPOX clusters are presented. Then, the stationary process flowsheet modeling techniques are detailed, and the coupling between interfaces is described.

2.1. Reactor Modelling

Two oxygen carriers were employed in the reactor models built in Scilab, which incorporated an in-house thermodynamic database (Patitug) for property calculations of the gas phase. The first reactor principle consists of gas switching reforming (GSR) using Nickel as an oxygen carrier, inspired in past studies from some of the authors [22]. The second reactor principle incorporates the novel oxygen carrier which achieves partial oxidation of methane, referred to henceforward as gas switching partial oxidation (GSPOX). For the solid property estimation, suitable data sources were employed [32,33]. The oxygen carrier used in the GSPOX schemes had the chemical composition $La_{0.85}Sr_{0.15}Fe_{0.95}Al_{0.05}O_3$. Generally, thermodynamic data for such compositions are scarce, therefore the specific heat

capacity was estimated based on literature data for species that represent the components in the fully oxidized and fully reduced states of the oxygen carrier, respectively. For the oxidized oxygen carrier, the specific heat capacity reported for $LaFeO_3$ was used [34]. The composition of the reduced oxygen carrier consisted of 50.2 wt.% La_2O_3, 23.0 wt.%. Fe and 26.8 wt.% $La_xSr_{2-x}Fe_yAl_{1-y}O_4$ [31]; the mixed oxide phase $La_xSr_{2-x}Fe_yAl_{1-y}O_4$ was assumed to possess the same physical properties as $LaFeO_3$. The specific heat capacity of the individual components was thus averaged using published data and interpolated across the operating temperature range of the reactor [32].

The specific enthalpy of reduced or oxidized species at each reactor temperature was estimated based on the experimental value for the partial oxidation of methane with the oxidized species, and equal to 222.25 kJ/mol of CH_4 at 900 °C [31], assuming an enthalpy origin of the reduced species at 298.15 K. Further property details of this oxygen carrier and cluster modeling assumptions are provided in Table A2 in Appendix A.

Each reactor has a 1 m diameter and an aspect ratio of 3, which resulted in fluidization velocities of approximately 0.6–0.8 m/s for operating temperatures between 900–1100 °C. A pressure drop of 0.5 bar in each reactor was assumed in all cases. With a similar approach as in [22], additional thermal mass in the form of steel rods was introduced in the reactor to mitigate the temperature variation across the GSR and GSPOX cycles. The steel rods were assumed to occupy 25% of the reactor volume for all simulations. The specific heat of the carbon steel rods was assumed from [35], constant in the range of reactor operating temperatures. The carbon steel rods did not actively participate in the redox reactions (such that gas would be converted or produced), but only acted as a medium for storing heat.

Both for GSR and GSPOX reactors, the dynamic molar species Equation (1) and energy Equation (2) balances are solved to determine the reactor profile (temperature and compositions) and outlet flows, assuming the fluidized bed behaves as a continuous stirred tank reactor (CSTR), in virtue of the high degree of mixing attained in industrial practice:

$$\frac{dn_k}{dt} = F_{in}y_{in,k} + F_{out}y_{out,k} + \sum_{r=1}^{R} v_{r,k}\xi_r \tag{1}$$

$$\frac{dT}{dt} = \frac{-F_{in}\sum_k y_{in,k}\int_{T_{in}}^{T} c_{p,k}dT + \sum_{r=1}^{R}\xi_r(-\Delta H_{r,T})}{\sum_k n_k c_{p,k}}. \tag{2}$$

The CSTR model assumes that both chemical and thermal equilibrium is reached. Thermal equilibrium is a realistic assumption in fluidized bed reactors and experimental work has shown that chemical equilibrium is also a reasonable approach for the highly reactive Ni-based oxygen carrier used in GSR [21]. The validity of this assumption is unknown for the GSPOX reactor, but, since the present study evaluates the potential of an ideal GSPOX oxygen carrier, it is assumed that this oxygen carrier also reacts fast enough to reach chemical equilibrium [31].

The energy balance is solved first and, making use of the ideal gas relationship, the instantaneous outlet flow F_{out} Equation (3) is determined to subsequently solve the species balance. In this way, Equations (1) and (2) are decoupled. A stiff ordinary differential equation (ode) solver is used for this purpose.

$$F_{out} = F_{in} + \sum_{R}^{k\in gases} v_{k,r}\xi_r + \frac{PV_{gas}}{RT^2}\frac{dT}{dt}. \tag{3}$$

The instantaneous outlet flows, compositions and temperatures from each step in the GSR and GSPOX cycles are averaged to deliver constant values to the stationary simulation. This is done on the assumption that a sufficiently large cluster of GS reactors will be used so that multiple reactors will operate in each reactor step at any given time. For instance, in the GSR model for H_2 production the cluster was designed with 7 reactors operating in the reforming step, 3 in oxidation and 3 in reduction at any given instant. When the outlet

streams from different reactors in each step were mixed, minimal transient fluctuations in flowrate, temperature and composition were achieved, in this way ensuring a stable operation of the downstream process units.

The results of the simulation led to mass balance relative errors in the order of around 0.1%. Due to the high degree of heat integration between the clusters and the stationary plant, besides the averaging of instantaneous outlets taking place, the process simulations were converged with a relative energy balance error below 0.5%.

2.1.1. Gas Switching Reforming

Analogously to previous work [22], full fuel conversion in the reduction was assumed and, to prevent kinetic limitations taking place at the end of this step, a minimum fraction (5%) of the oxygen carrier in its oxidized state is specified. The carrier is then fully reduced during the subsequent long reforming step. After the reforming, the degree of oxygen carrier oxidation with the air stream was set to 30%, while the total airflow rate was selected to avoid any accumulation of O_2 in the reactor. The heating value routed to the reduction inlet is controlled to ensure the autothermal operation by tuning the overall steam to carbon ratio at the reforming feed.

The oxygen carrier in the GSR is based on Nickel, with the formulation taken from Abad et al. [36]. As illustrated in Figure 1, the reactor operates in a cycle consisting of reforming (REF), oxidation (OX) and reduction (RED). The kinetic equations that determine the rate of reaction in each step are expressed in Table 1 below. A value of 0.01 for the relaxation time constant τ was selected to reach full conversion (or equilibrium) of the reactants in the reactor volume.

Table 1. Reactions and kinetic expression for GSR.

Step	Reaction	Kinetics
REF	$CH_4 + H_2O \leftrightarrow CO + 3H_2$	$R_{SMR} = \frac{1}{\tau}\left(p_{CH_4}p_{H_2O} - \frac{p_{CO}p_{H_2}^3}{K_{SMR}}\right)$
	$CO + H_2O \leftrightarrow CO_2 + H_2$	$R_{WGS} = \frac{1}{\tau}\left(p_{CO}p_{H_2O} - \frac{p_{CO_2}p_{H_2O}}{K_{WGS}}\right)$
OX	$O_2 + 2Ni \rightarrow 2NiO$	$R_{O_2} = \frac{1}{\tau}n_{O_2}n_{Ni}$
RED	$CH_4 + 4NiO \rightarrow 4Ni + CO_2 + 2H_2O$	$R_{CH_4} = \frac{1}{\tau}n_{CH_4}n_{NiO}$
	$H_2 + NiO \rightarrow Ni + H_2O$	$R_{H_2} = \frac{1}{\tau}n_{H_2}n_{NiO}$
	$CO + NiO \rightarrow Ni + CO_2$	$R_{CO} = \frac{1}{\tau}n_{CO}n_{NiO}$

An illustration of the GSR reactor profile (product stream composition and temperature) corresponding to one of the H_2 plant simulations is presented in Figure 3.

The equilibrium constants for the WGS and SMR reactions are a function of thermodynamic properties and dependent on temperature [37], as represented by Equations (4) and (5).

$$K_{SMR} = 1.2 \times 10^{13} e^{\left(\frac{-223{,}080}{RT}\right)} \quad (4)$$

$$K_{WGS} = 0.0177 e^{\left(\frac{36{,}850}{RT}\right)}. \quad (5)$$

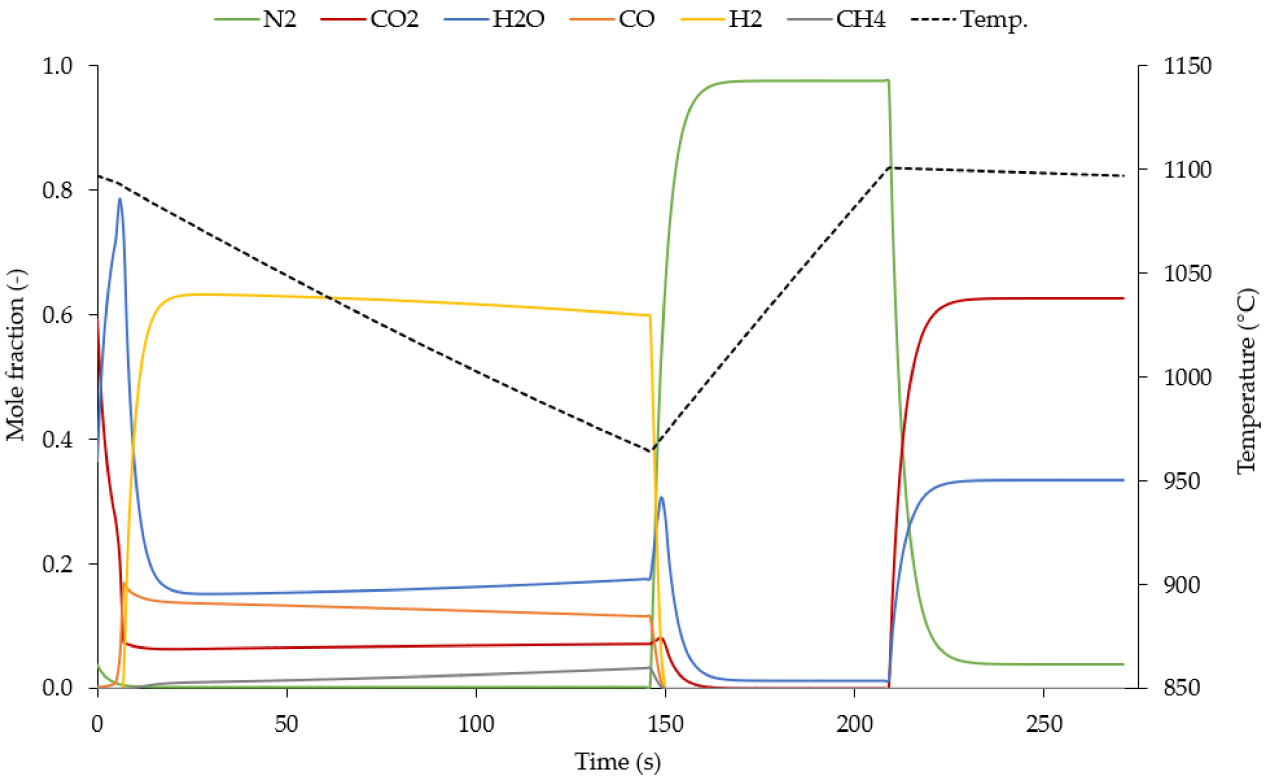

Figure 3. GSR reactor cycle composition and temperature profile. (REF: 0–146.3 s, OX: 146.3–209.0 s, RED: 209.0–271.7 s).

2.1.2. Gas Switching Partial Oxidation

The modeling of the La-Fe-based oxygen carrier for GSPOX is based on the promising experimental results obtained in [31]. Good performance has also been achieved in a fluidized bed, increasing confidence in the application to gas switching reactors [38]. The original oxygen carrier possesses an oxygen storage capacity of ~9 wt.% and thermodynamic properties such that ~96.5% of its redox-active lattice oxygen is selective for the partial oxidation of methane to syngas (in the reduction step) and ~95% of steam (or CO_2) can be converted to H_2 (or CO), in the oxidation step. The aim is to develop and assess the application of this oxygen carrier in an H_2 production plant, benchmarking it against the former GSR plant and the reference technology: SMR process. For this purpose, certain ideal performance assumptions have been taken, as further detailed below.

The chemical reactions and kinetic expressions considered for each step are presented in Table 2 for the GSPOX reactor, where the fully oxidized oxygen carrier is denoted by XO, while the reduced oxygen carrier is referred to as X.

Table 2. Reactions and kinetic expressions for GSPOX.

Step	Reaction	Kinetics
POX and REF/WS	$CH_4 + 0.74XO_{1.35} \rightarrow 0.74X + CO + 2H_2$	$R_{CH_4} = \frac{1}{\tau} n_{CH_4} n_{XO}$
	$0.74X + CO_2 \leftrightarrow 0.74XO_{1.35} + CO$	$R_{CO_2} = \frac{1}{\tau}\left(y_{CO_2} - y_{CO_2,eq}\right) n_{gas} n_X$
	$0.74X + H_2O \leftrightarrow 0.74XO_{1.35} + H_2$	$R_{H_2O} = \frac{1}{\tau}\left(y_{H_2O} - y_{H_2O,eq}\right) n_{gas} n_X$
OX	$1.48X + O_2 \rightarrow 1.48XO_{1.35}$	$R_{O_2} = \frac{1}{\tau} n_{O_2} n_X$
RED	$0.74XO_{1.35} + H_2 \rightarrow 0.74X + H_2O$	$R_{H_2} = \frac{1}{\tau} n_{H_2} n_{XO}$
	$0.74XO_{1.35} + CO \rightarrow 0.74X + CO_2$	$R_{CO} = \frac{1}{\tau} n_{CO} n_{XO}$
	$CH_4 + 2.96XO_{1.35} \rightarrow 2.96X + CO_2 + 2H_2O$	$R_{CH_4} = \frac{1}{\tau} n_{CH_4} n_{XO}$

The proposed cycle includes a two-step reduction. In the first step, the oxygen carrier shows full selectivity to CO_2 and H_2O and fully oxidizes all fuel gases fed to the reactor. In the second step, the oxygen carrier has 95% selectivity to H_2 and CO, by partially oxidizing CH_4 and reducing H_2O or CO_2 fed to the reactor. It is assumed that the transition point between these two steps (i.e., to what degree the oxygen carrier is reduced when the selectivity of the oxygen carrier changes from total to partial oxidation) can be tuned according to the requirements of the process, e.g., by decreasing the ratio of La:Sr in the oxygen carrier [31], or by adding other combustion oxygen carriers such as ilmenite to the formulation [39]. The modeling results reveal that approximately half of the lattice oxygen that is consumed during reduction (case dependent) must fully oxidize the fuel to achieve adequate step lengths. Since the overall degree of oxygen carrier reduction was limited in all cases below 70%, and due to the higher resistance of these materials to carbon deposition [40], it was neglected in the kinetic model.

In the partial oxidation step (POX) two moles of H_2 are present per mole of CO produced. Unlike in the reforming step in the GSR, a large flow of steam is not required to ensure high methane conversion. An oxygen carrier conversion of 30% in addition to that for the reduction step (where full combustion of the fuel takes place) is specified for the POX step. For GSPOX H_2 production plants, in the subsequent reforming step (REF), a methane-steam feed with a molar ratio of 1 is fed to the reactor, thereby attaining more H_2 in the outlet (ratio of 3:1). During the reforming step, a negligible carrier conversion is observed due to the equimolar feed of methane and water that cause forward and backward reactions to take place at identical rates. The following oxidation step is carried out similarly to the GSR reactor, with only sufficient air to fully re-oxidize the carrier (no O_2 slippage). Finally, in the reduction step (RED), the PSA off-gas fuel is completely combusted to CO_2 and H_2O.

In Figure 4, a case corresponding to the GSPOX model designed for H_2 production is presented, whereas in Figure 5, a case for H_2-power co-production is shown. In Figure 5, air is introduced in the oxidation step in excess, to allow subsequent extra firing to reach high gas turbine (GT) combustor outlet temperatures (COT) to maximize efficiency. The low-carbon fuel for the extra firing is generated by operating the water splitting (WS) step with a steam sweep (as opposed to the equimolar methane-steam feed to the reforming step), in order to obtain a relatively pure H_2 output. This latter strategy is not advisable for H_2 production only, since the H_2 purity of the product stream is approximately 90%, and therefore it would still require a cooldown and purification sequence, neglecting potential efficiency gains whilst increasing operational complexity. It was therefore decided to carry out the reforming as described earlier and mix the process stream outlets from the partial oxidation and reforming steps in Figure 4 before introducing them to the downstream WGS reactors.

For the H_2-power coproduction reactor profile (Figure 5), the maximum reactor temperature is attained in the oxidation step at the point where the carrier becomes fully oxidized, after which the reactor cools down and the O_2 concertation begins to increase. The mass flow rate of air is manipulated from the stationary simulation to reach autothermal operation (energy conservation across the cycle), while the initial reactor temperature was iteratively varied to reach the specified maximum temperature. On the other hand, the degree of oxygen carrier reoxidation during the WS step was manipulated in order to produce sufficient H_2 to reach the nominal COT value upon combustion with the O_2 depleted air stream from the oxidation step outlet.

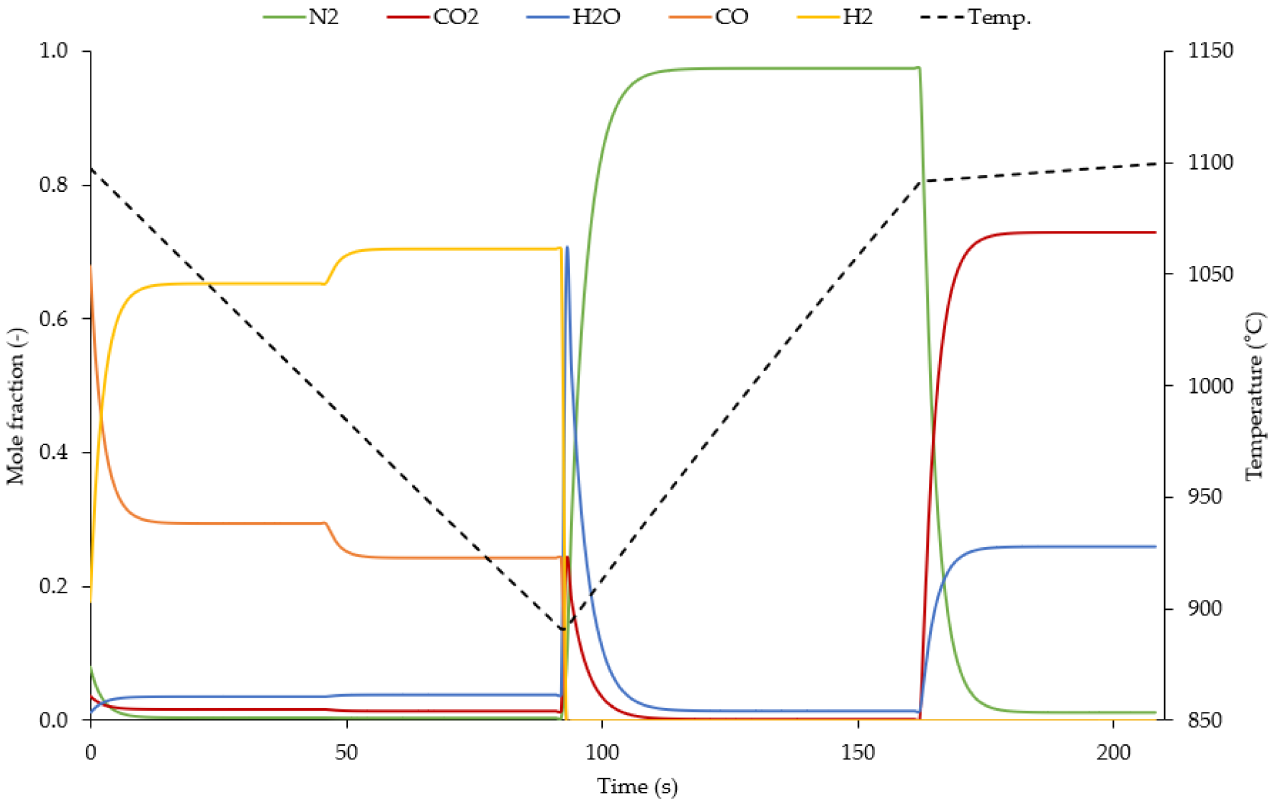

Figure 4. GSPOX reactor cycle composition and temperature profile for an H_2 plant case. (POX: 0–46.4 s, REF: 46.4–92.7 s, OX: 92.7–162.3 s, RED: 162.3–208.6 s).

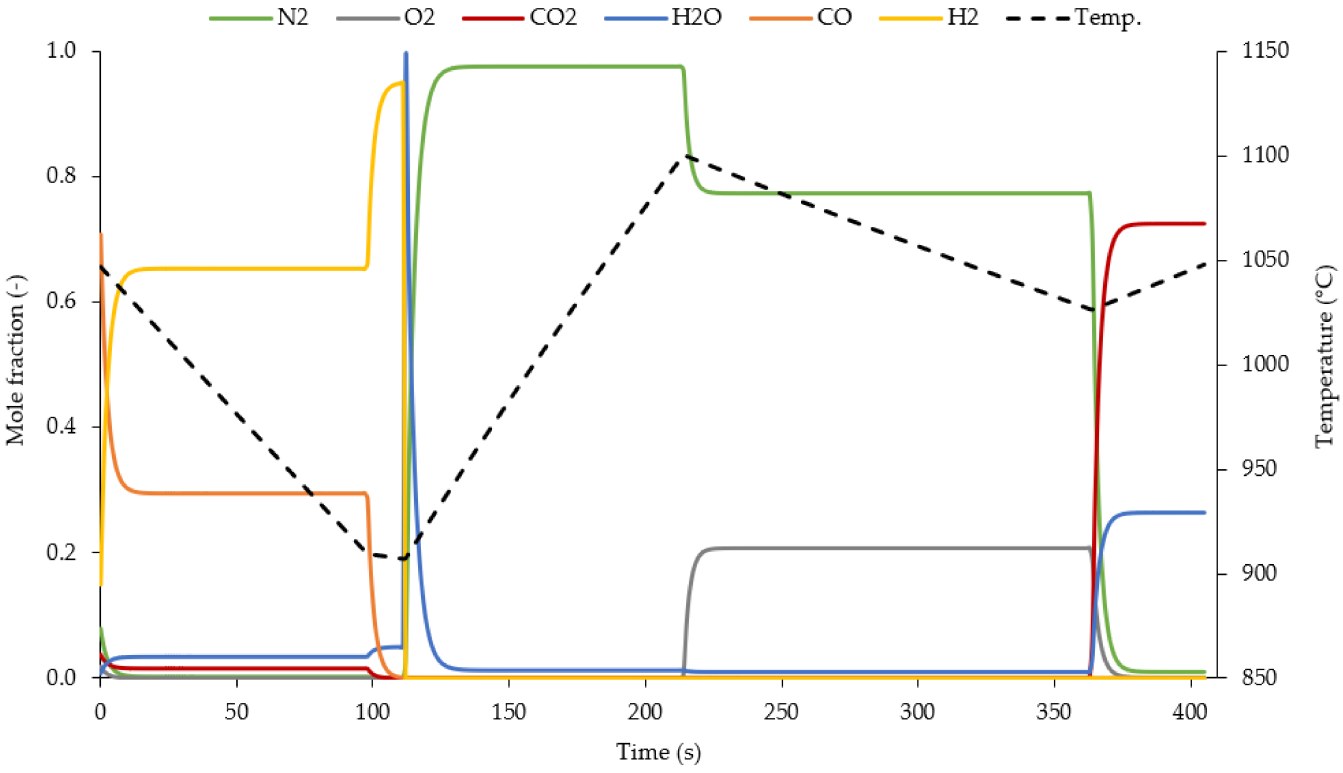

Figure 5. GSPOX reactor cycle composition and temperature profile for an H_2-power co-production plant case. (POX: 0–97.8 s, WS: 97.8–111.7 s, OX: 111.7–363.1 s, RED: 363.1–405.0 s).

The mole fraction at equilibrium of CO_2 and H_2O for the kinetic expressions in Table 2 is determined as a function of the specified selectivity to CO and H_2 (assumed conservatively to be 95%) and the actual mole fraction of each gas species in the reactor at any given time, as shown in Equations (6) and (7). Where s_k indicates the selectivity towards a specific component k. Reactions taking place in reduction and oxidation steps proceed to completion, while only methane in the partial oxidation step is fully converted.

$$\frac{y_{H_2}}{y_{H_2} + y_{H_2O,eq}} = s_{H_2} \quad (6)$$

$$\frac{y_{co}}{y_{co} + y_{co_2,eq}} = s_{co}. \quad (7)$$

2.2. Process Modelling

The averaged outlets from each cluster step are introduced in the stationary process simulator by means of a CAPE-OPEN unit operation. Similarly, the feed streams to the reactors are taken from the plant model. The process flowsheets were developed with consistent modeling assumptions to similar studies and are further detailed in Table A1 in Appendix A. For the H_2-power GSPOX plants, two representative gas turbine technologies employed for base-load power production [41,42] were calibrated using natural gas fuel. The equipment efficiencies and combustor performance with representative blade cooling technology from each turbomachine were specified in the GT units of the H_2-power plants. The models were built in Unisim Design R451 from Honeywell, using the Peng Robinson equation of state for thermodynamic property calculations, and ASME steam tables for water and steam streams.

2.2.1. SMR H_2 Plant without CO_2 Capture

The SMR plant has been extensively reviewed in earlier research. The present work introduces an SMR concept based on the technological features described in [11,22,43], in order to provide a benchmark process developed with the same simulation tool as the novel H_2-power plant concepts. A natural gas heat input of 129 MW (LHV) is considered as a calculation basis for all the models developed.

A process diagram of the SMR plant is shown in Figure 6. The natural gas feed is introduced in a preheater with the reformer exhaust gas. After desulphurization and pre-reforming to eliminate C2+ species, the natural gas is heated to 620 °C fed to the fired tube reformer (FTR) with a steam-to-carbon ratio (S/C) of 2.7. Approximately 87.0% of methane conversion is achieved in the outcoming syngas at 890 °C, a limiting temperature to avoid overheating and failure of the catalyst-packed tubes exposed to the flame. After cooling in a series of heat exchangers producing HP steam at 92 bar and 485 °C, the CO present is converted CO_2 by steam shift, producing more H_2. Once the H_2-rich syngas is cooled down to ambient temperature, it is routed to the PSA unit where the H_2 product is retrieved, while the off-gas is used as fuel in the burner in the FTR furnace.

In order to provide sufficient heat for the endothermic reforming reaction to take place, a small portion of the original fuel after the desulphurizer is also combusted with air (introduced with a 15% O_2 excess) in the FTR. The exhaust gases at low pressure and high temperature (1010 °C) are used to preheat the incoming feed streams and to generate more HP superheated steam. A small air blower is needed to overcome the pressure losses of the heat recovery network.

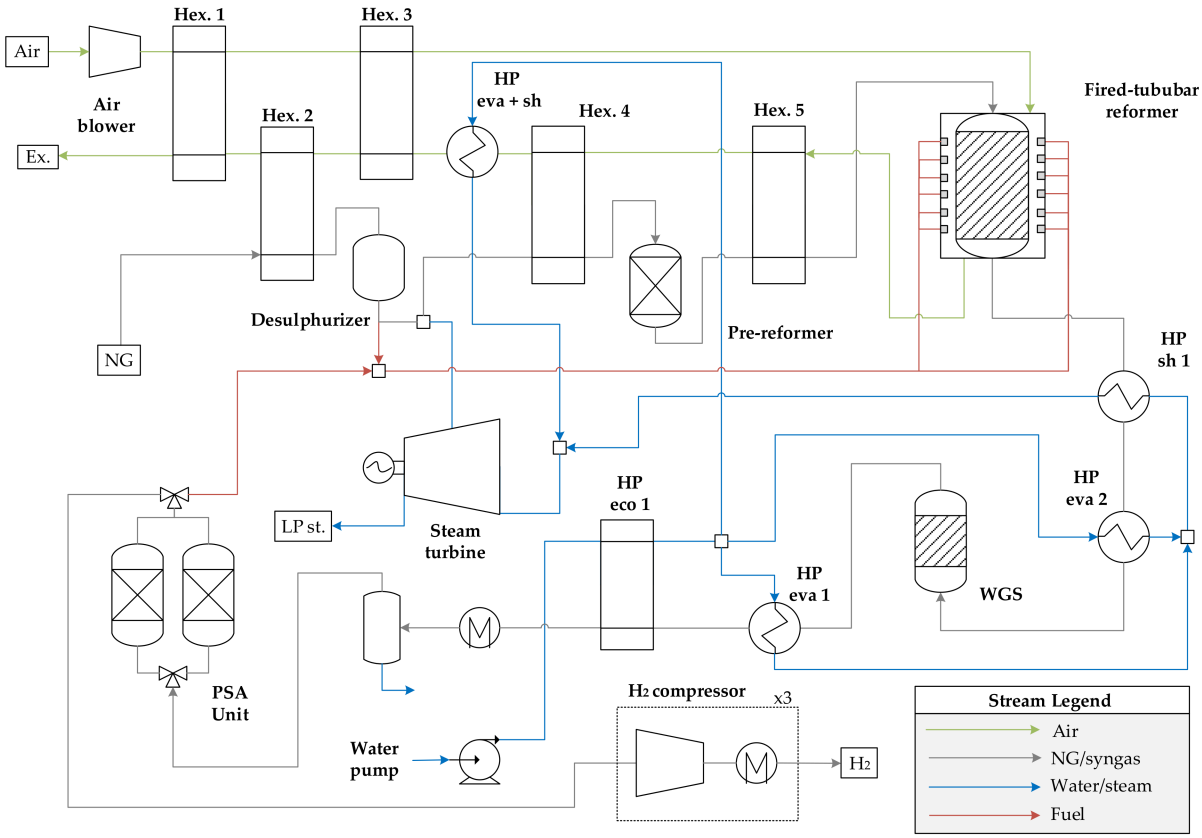

Figure 6. Process diagram of the SMR plant without CO_2 capture.

2.2.2. SMR H_2 Plant with MDEA Absorption CO_2 Capture

For completeness of the benchmarking plants, a CO_2 capture SMR plant was developed using an absorption unit with MDEA prior to the PSA, in order to remove 95% of the CO_2 present in the shifted syngas stream. A process diagram is provided in Figure 7. The MDEA section was modeled with a dedicated thermodynamic model (DBR Amine Package: Kent-Eisenberg) facilitated by Honeywell to accurately represent the chemical absorption process. The use of a chemical solvent is suitable for the intermediate partial pressures of CO_2 at the inlet stream to the absorption unit. Furthermore, MDEA presents a low regeneration heat requirement amongst amine-based solvents: The Unisim model with partial flash solvent regeneration predicted a value of 1.07 MJ_{th} per kg of CO_2, very closely matching the values reported in [44]. The integration of conventional CO_2 capture through amine absorption has several implications: the S/C ratio was increased to 4,as in [11,43], to achieve maximum methane conversion in the tubular reformer (92.5%), while a second, low-temperature shift (LTS) unit is added to fully convert the CO present in the syngas produced. Furthermore, a portion of the purified H_2 stream after the MDEA unit must be employed in the burner to satisfy the energy balance without increasing CO_2 emissions. Lastly, since the steam demand is large, all the steam produced in the heat recovery systems is either employed to reach the required S/C ratio in the reformer or in the MDEA stripper column for solvent regeneration. A dedicated LP boiler after the LTS unit is used to fulfill the LP steam demand. The resulting decreased steam turbine output and the extra auxiliary consumption imposed by the 5-stage intercooled CO_2 compressor and downstream supercritical CO_2 pump results in negative net electricity production for this plant. Both H_2 and CO_2 products are delivered at a pressure of 150 bar. Given that the GSR and GSPOX H_2 plants are assumed to import a substantial amount of electricity, the SMR with MDEA CO_2 capture model was designed to rely as well on electricity imports to enable a fair comparison, and only sufficient steam is raised to satisfy the S/C require-

ments. Therefore, the steam turbine (ST) output will decrease considerably, but less pure H_2 product will be combusted in the reformer, ultimately leading to higher H_2 efficiencies and lower penalties than in the case where the steam turbine is operated to satisfy the plant energy demand.

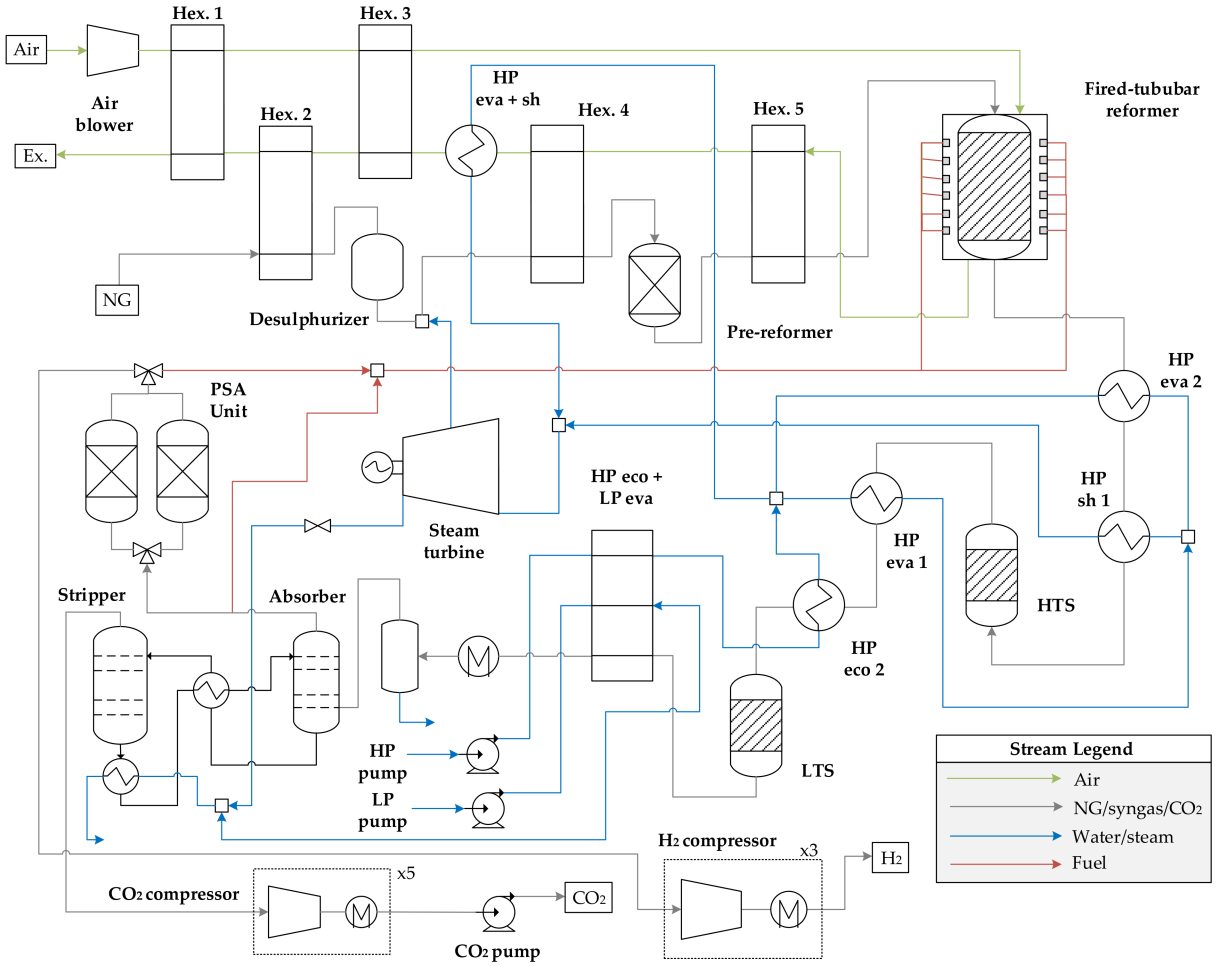

Figure 7. Process diagram of the SMR H_2 plant with MDEA absorption CO_2 capture.

2.2.3. GSR H_2 Plant

The GSR H_2 plant is modeled following the guidelines provided in Nazir et al. [22]. Due to the higher temperatures reached (up to 1100 °C at the end of the reduction and beginning of the reforming stage) in the flameless combustion attained with the chemical looping principle, a lower S/C ratio is needed to achieve high methane conversion relative to the SMR models. Precisely this parameter is tuned to obtain sufficient heating value in the PSA off-gas, which is routed to the reduction step after compression and heating to satisfy the cluster energy balance. Somewhat higher H_2 efficiencies are obtained in the present work relative to the original work [22] as a result of improved heat integration. Thus, a higher fraction of the fuel heating value is preserved as H_2 and not combusted to maintain reactor operating temperatures. The elements of which the GSR-H_2 plant consists are practically the same as the GSPOX-H_2 plant described in the next section and illustrated in Figure 8. The base case reactor operating pressure is the same as in the SMR plants (32.7 bar) and it was assumed that the air and PSA-off-gas stream pressurization was carried out in a single adiabatic compressor stage. The PSA separation performance was represented using the correlation derived by Nazir [22], assuming 100% purity of the H_2 product stream. As represented in Equation (A1) in Appendix A, the hydrogen recovery

is directly related to the pressure relation between the adsorption and desorption stages, which is linked to the off-gas compressor auxiliary power for the plants integrating GS clusters. H_2 recoveries beyond 80% are achieved for all the plants investigated.

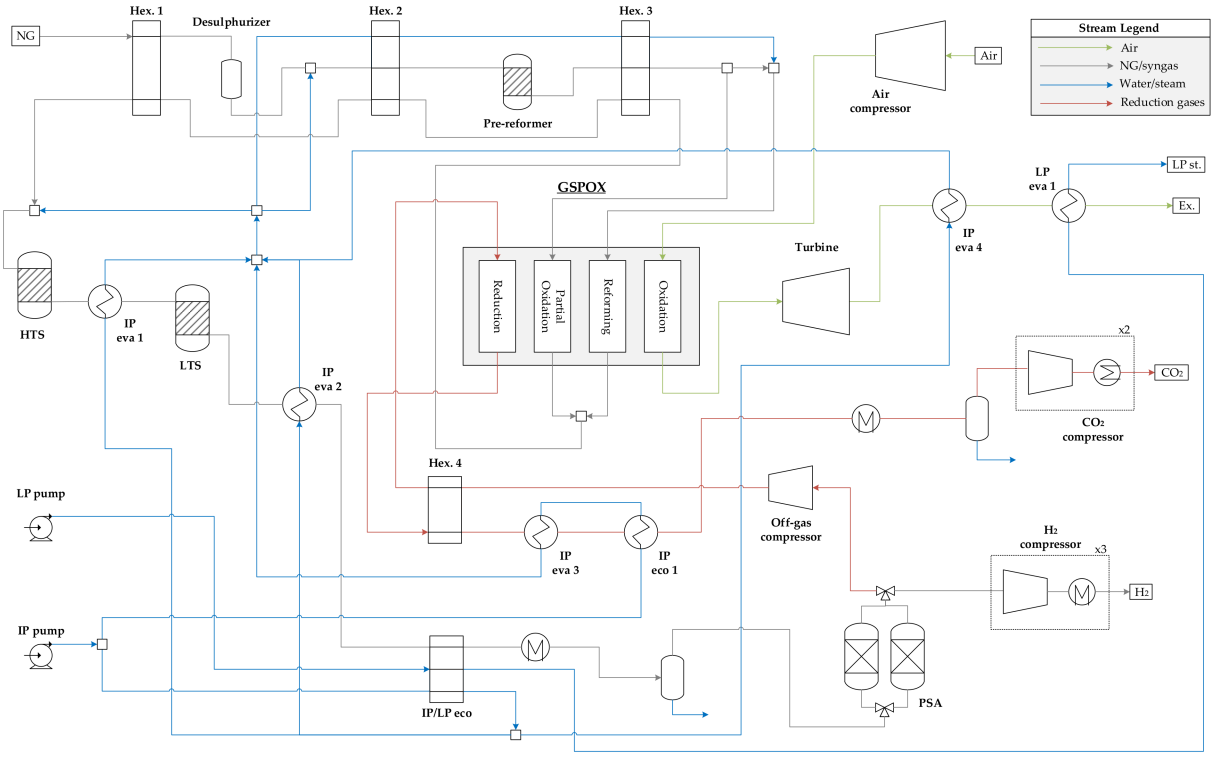

Figure 8. Process diagram of the GSPOX H_2 plant.

Some considerations will be made regarding the heat integration for the benchmark and GS-based plants. For the fired tubular reforming SMR plants, on the combustion gases side, the low pressure of the stack gases will result in a small heat transfer coefficient, which leads to large temperature differences with respect to the incoming natural gas feed, achieving a relatively low preheating temperature. On the syngas side, the steam generation network is arranged in such a way as to avoid steam superheating with the high-temperature reformer outlet syngas, preventing an environment that would cause exchanger tube failure due to metal dusting [45]. On the other hand, the temperature approaches considered in the GS plants allow for a considerably higher heat recovery performance. The pressurized conditions of the streams found in the GSR and GSPOX clusters maximize the heat transfer coefficient relative to the reference plants, enabling closer temperature approaches. Special precautions may be required for the exchangers which preheat the mixed steam and gas streams to the GS clusters with the high-temperature syngas product, despite the fact that the steam pressures (25–40 bar) are notably below the design values of the conventional SMR processes (>100 bar). The PSA off-gas recuperator with the GS reduction outlet is an item that will also require advanced heat exchanger design [46]. The potential to achieve higher preheating temperatures inherent to the GS cluster operation represents an important feature to accomplish the high H_2 efficiency conversions attained in the concepts integrating this technology.

2.2.4. GSPOX H_2 Plant

The process configuration for the GSPOX-H_2 concept is depicted in Figure 8 It is assumed that the pre-reformer catalyst can cope with a decreased steam to carbon ratio, and it was specified to achieve a 99.9% equilibrium conversion of C2+ species. It is noteworthy to mention that the GSPOX oxygen carrier is likely to be able to handle higher

molecular weight hydrocarbons, but in order to avoid greater modeling complexity in the Scilab code (additional kinetic expressions and increased n° of differential equations), the C2+ components were converted prior to the GSPOX. The outlets of the partial oxidation and reforming steps are mixed and cooled down in Hex1, Hex2 and Hex3, prior to a water gas shift conversion in two stages. Intermediate Pressure (IP) steam is generated in boilers with the heat of reaction; it is employed in the pre-reformer and the reforming steps of the GSPOX and also added to the feed of the High-Temperature Shift (HTS) bed. After cooling to ambient temperature, the shifted syngas is routed to the PSA unit, where a pure H_2 stream is compressed to 150 bar and delivered as a product. The PSA off-gas at low pressure is recompressed and sent to the reduction step feed. By tuning the steam input to the HTS bed the CO conversion is controlled. In this way, the amount of heating value remaining in the PSA off-gas is manipulated to operate the GSPOX reactors autothermally. The reduction gases outlet from the GSPOX are used to preheat the incoming PSA off-gas, and further cooled producing more IP steam. The off-gas temperature inlet to the reduction step was manipulated to satisfy the steam demand balance, in such a way that all process models are self-sufficient.

The oxidation section presents a simple power unit, in which the compressor delivers air to the oxidation step of the GSPOX and a low turbine inlet temperature (TIT) of around 1000 °C retrieves some useful electricity for the plant. No blade cooling was considered for this case. Due to the large pressure ratio of the turbine and low TIT, the turbine outlet temperature (TOT) is relatively low. An IP evaporator and LP evaporator produce steam with the remaining heat of the air stream. The IP steam is used within the plant, but the LP steam must be exported as a product.

2.2.5. GSPOX H_2-Power Plant

As described earlier, the GSPOX H_2-power plant can simultaneously produce H_2 and electricity, by operating the reforming step of the cluster with a water sweep. A similar option is possible with the GSR, withdrawing some H_2 product for extra firing, but this hydrogen would need to be separated from the syngas stream via larger WGS and PSA units instead of being directly produced via water splitting as in the GSPOX process. In addition, if the oxidation step is operated with excess air, the reactor cool-down taking place after carrier full oxidation will reduce the subsequent reforming step temperature, thereby increasing the steam requirement for comparable methane conversion.

The basic layout of this concept is represented in Figure 9. The essential differences with respect to the H_2 only production plant are (1) the use of a water sweep in the reforming step to produce a semi-pure H_2 stream for extra firing, (2) the avoidance of a WGS step after the partial oxidation and heat recovery sections, and (3) a more complex power cycle in the oxidation section. By removing the WGS units, a lower amount of the heating value originally present in the natural gas is withdrawn as H_2 in the PSA unit. Consequently, a larger flow rate of air is heated in the GSPOX reactor, producing more electricity upon expansion. From an efficiency perspective, removal of the WGS reactors also avoids degrading a significant fraction of the fuel heating value to relatively low-grade heat via the exothermic WGS reaction. Since the PSA off-gas is now much richer in volatile components (CO, H_2) relative to the H_2 plant (with a large presence of CO_2 and H_2O from the shift), the PSA-off-gas compressor was split into two intercooled stages, to reduce the safety concerns of an excessive adiabatic temperature rise.

The power cycle indicated in Figure 9 is specifically integrated with the rest of the plant. It integrates hot water/LP steam produced from low-temperature heat recovery units of the reduction and partial oxidation streams to effectively use them for extra electricity generation. Moreover, the cycle is designed to satisfy the internal steam demand, delivering IP steam to the reforming step and pre-reformer as required. In this way, the potential disadvantage in the case of no suitable end-use for LP steam production in the H_2-only plants is entirely avoided. Given the uncertainty of the scale of the devised concepts using GS technology, several power cycles may prove competitive, depending on different factors

such as plant location, natural gas heat input, price of electricity and H_2 etc. However, for this study, only a combined power cycle is considered to evaluate the potential benefits of the H_2-power GSPOX configuration relative to the H_2-only configuration.

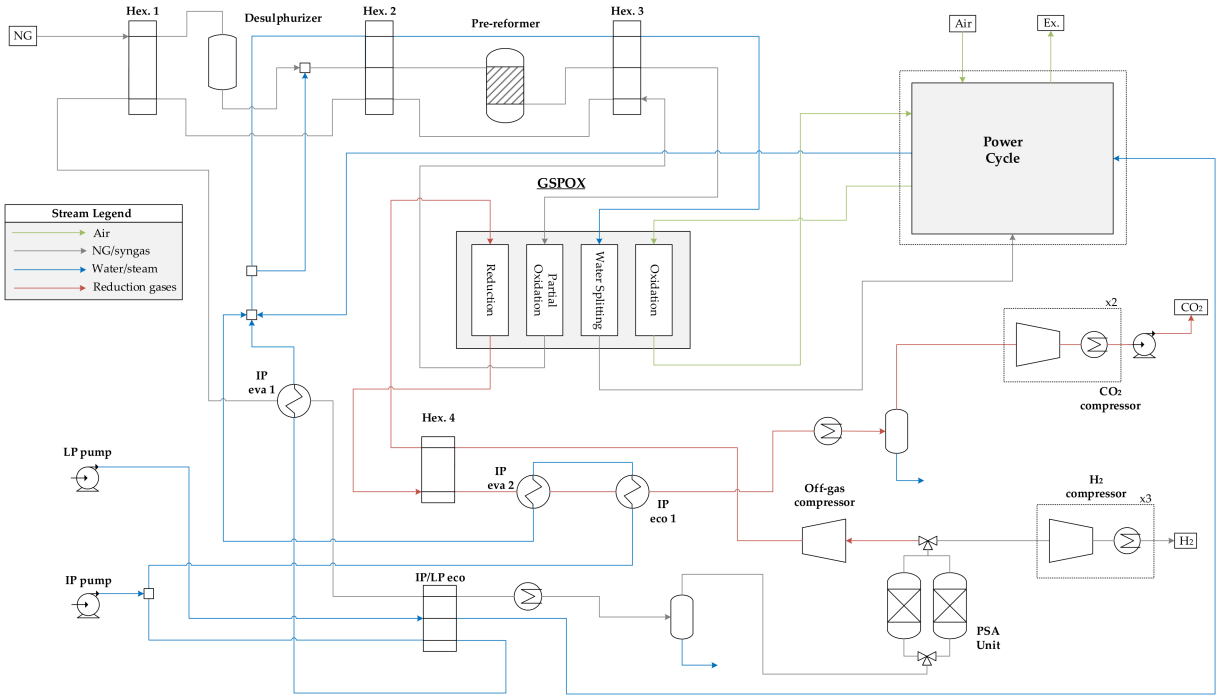

Figure 9. Process diagram of the generic GPSPOX H_2-power concept.

In such a combined power cycle, the gas turbine integrated with the GSPOX oxidation and water splitting steps delivers a high-temperature exhaust gas stream to a steam cycle, to produce additional electricity. This configuration is depicted in Figure 10, where only the oxidation and water splitting sections of the GSPOX cluster unit are shown and process equipment within the dotted lines refer to the units appearing in the block "power cycle" in Figure 9.

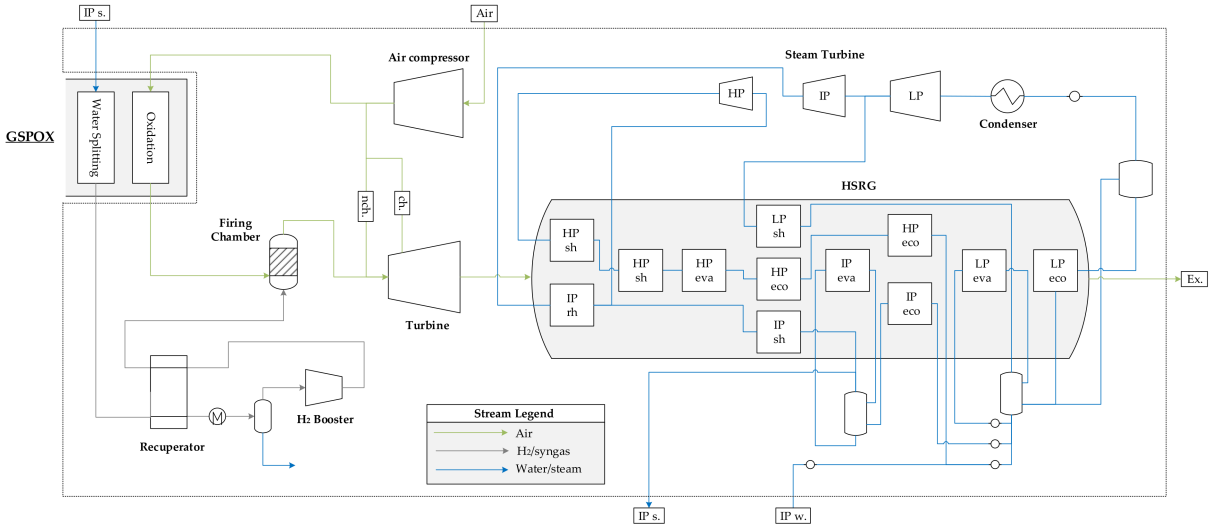

Figure 10. Process diagram of the combined cycle for the oxidation section of the GSPOX H_2-power plant.

The gas turbine elements associated with the GSPOX H_2-power plants are representative of two industrial turbomachines employed for power production in combined cycles. It is noted that the power systems integrated into these processes are not specifically the actual GTs, but rather incorporate several defining technological features to represent that technology level. Therefore, the case incorporating the technological features of the H-class turbines is henceforward denoted as "Advanced", while the case with the F-class characteristics is referred to as "Current", to potentially avoid confusion with the actual machines. A simplified gas turbine model as depicted in Figure A1 in Appendix A using reference values for combustor outlet temperature (COT), turbine inlet temperature (TIT) and turbine outlet temperature (TOT) is calibrated, specifying the compression and expansion polytropic efficiencies to reach the known reference open cycle efficiency. Table A3 in Appendix A shows the results of the calibration for the two types of turbomachines employed, as well as the reference values for each GT open cycle.

A lumped blade cooling flow model where the coolant is taken from compressor discharge and injected in the hot gas path at two points is developed, similar to what is proposed in [47]. Coolant addition after the combustor represents the refrigeration requirements of the 1st stator (non-chargeable cooling flow), while the rotor and subsequent rows (chargeable cooling flow) is added at 1/3 of the expansion path. For calibration, each coolant flow is varied to reach the specific TIT and TOT of the GT. In this way, the b values for stator and rotor shown in Equations (A2) and (A3) respectively in Appendix A, given a certain maximum blade temperature, are determined for each GT. When integrating an analogous technological cycle in the H_2-power plants, the cooling flows are predicted with a reasonable level of accuracy, assuming constant b values and open loop convective cooling as heat transfer model. Given that the COT values are the same as those of the reference machines, the cooling flow fractions do not deviate largely from the NG fired model. A pressure drop after the mixing of coolant and gas streams is considered to represent efficiency losses associated with this mixing, proportional to the coolant to hot gas ratio φ as suggested in [48], and shown in Equation (A4) in the Appendix A. A more detailed derivation of the heat exchange effects between coolant and hot gas path in the blade as well as different cooling mechanisms is described by Sanjay et al. [49]. A precise prediction of coolant flows with injection at several stages of the expansion path is provided by Chiesa and Macchi for deployable natural gas combined cycles [50]. For the conceptual design of H_2-power processes at a low technology readiness level (TLR) and the current state of development, requiring tailor-made turbomachinery components to reach attractive efficiencies, the simplified approach is considered reasonable. Indeed, the reference gas turbines are taken from combined cycle applications [41,51], whose heat rate is substantially above the natural gas heat input to the plants presented in this study.

The air compressor is therefore operated at the reference pressure ratio of each specific GT. The H_2 rich stream produced in the GSPOX water splitting stage is cooled down in a recuperator and then compressed in a booster and reheated. This is done to allow for an overpressure of 10 bar for the H_2-rich fuel stream prior to extra firing in the combustor chamber. The fuel must be delivered at sufficient pressure to the combustor by means of multiple fuel injectors to achieve a turbulent mixing between the rich H_2 fuel and hot depleted air from the GSPOX, leading to a swirling flow, which limits the flame temperature (to reduce NOx formation to acceptable limits), while avoiding the risk of flashback. An embodiment of the concept assumed here has been presented and experimentally tested in [52]. Small fluctuations in H_2 flow during valve switch in the WS stage that would affect combustion performance can be mitigated by pulsating water/steam addition at the recuperator inlet, although this was not accounted for in the plant simulation as the transient model delivers averaged values. Due to the larger number of reactors in the oxidation stage, the dimensionless flow rate variations of the blended oxidation outlet resulted in values below 1%, ensuring safe turbine operation [53].

Finally, the heat recovery steam generator unit (HSRG) of the steam cycle is the typical efficient design with three pressure levels and intermediate reheat previously modeled by

the authors [54]. Further modeling assumptions for this section are shown in Table A4 in Appendix A.

2.3. Plant Performance Indicators

To assess the performance in terms of efficiency and emissions of the different H_2-power production processes, several indicators are defined in this section. The H_2-power production plant can be envisaged as represented in Figure 11, attending to the products and by-products derived from it.

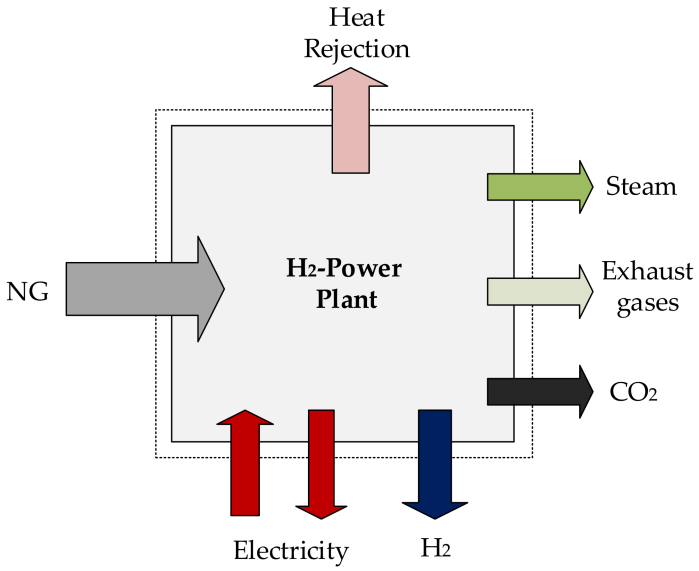

Figure 11. Simplified layout of the H_2-power plant.

The H_2 efficiency η_{H_2} in Equation (8) is determined as the relation between the heating value output of the H_2 stream and the heating value of the natural gas feed. However, this plant metric falls short to evaluate the electricity and steam demand or production that may take place in each of the plants. To fully account for these items, the equivalent natural gas feed $\dot{m}_{NG,eq}$ is calculated by subtracting (or adding) to the original feed the corresponding amount that would be required to generate the same quantity of steam or electricity as the current plant is exporting or importing, given a predefined benchmark efficiency for such production, as represented in Equation (9). In this way, a homogenous or equivalent efficiency $\eta_{H_2,eq}$ is defined in Equation (10). In previous works [22], it was shown that GSR H_2 concepts are reliant on electricity imports. On the other hand, it is frequent that substantial LP steam is produced as well. On some occasions, this steam can be utilized by other processes, and is accounted for in the equivalent efficiency calculation. However, it may be the case that there is no useful application for this steam, therefore the equivalent efficiency is recalculated accounting only for the electricity by-product (or import thereof), and denoted by a superscript in Equations (11) and (12).

$$\eta_{H_2} = \frac{\dot{m}_{H_2} LHV_{H_2}}{\dot{m}_{NG} LHV_{NG}} \tag{8}$$

$$\dot{m}_{NG,eq} = \left(\dot{m}_{NG} LHV_{NG} - \frac{\dot{W}_{el}}{\eta_{el}} - \frac{\dot{Q}_{th}}{\eta_{th}} \right) / LHV_{NG} \tag{9}$$

$$\eta_{H_2,eq} = \frac{\dot{m}_{H_2} LHV_{H_2}}{\dot{m}_{NG,eq} LHV_{NG}} \tag{10}$$

$$\dot{m}'_{NG,eq} = \left(\dot{m}_{NG} LHV_{NG} - \frac{\dot{W}_e}{\eta_e} \right) / LHV_{NG} \tag{11}$$

$$\eta'_{H_2,eq} = \frac{\dot{m}_{H_2} LHV_{H_2}}{\dot{m}'_{NG,eq} LHV_{NG}}. \tag{12}$$

In terms of CO_2 emissions performance, a similar approach is followed. The specific emissions E_{CO_2} calculated by Equation (13) are given in g of CO_2 per MJ of H_2 product. Alongside this, the capture ratio CC is the relation of the mass flow rate of CO_2 that is captured divided by the CO_2 intensity of the fuel E_{NG} as shown in Equation (16). When considering equivalent emissions $E_{CO_2,eq}$, the corresponding intensity of emissions avoided, derived from an alternative benchmark process for steam E_{th} and electricity production E_{el}, are accounted for and presented in Equation (14). The CO_2 avoidance is consequently defined by Equations (17) and (18) when steam is or is not considered as a useful product, respectively. Finally, the Specific Primary Energy Consumption of CO_2 Avoided ($SPECCA$) of every concept with CO_2 capture is calculated using the equivalent efficiency and emissions of the unabated SMR process as reference plant, as shown in Equation (19). This parameter gives an indication of the original fuel heating value that must be invested due to the integration of a CO_2 capture technology in the plant.

$$E_{CO_2} = \frac{\dot{m}_{CO_2,emit.}}{\dot{m}_{H_2} LHV_{H_2}} \tag{13}$$

$$E_{CO_2,eq} = \frac{\dot{m}_{CO_2,emit.} - E_{th}\dot{Q}_{th} - E_{el}\dot{W}_{el}}{\dot{m}_{H_2} LHV_{H_2}} \tag{14}$$

$$E'_{CO_2,eq} = \frac{\dot{m}_{CO_2,emit.} - E_{el}\dot{W}_{el}}{\dot{m}_{H_2} LHV_{H_2}} \tag{15}$$

$$CC = \frac{\dot{m}_{CO_2,\ capt.}}{\dot{m}_{NG} LHV_{NG} E_{NG}} \tag{16}$$

$$CA = \frac{\dot{m}_{CO_2,capt.}}{E_{NG}\dot{m}_{NG} LHV_{NG} - E_{th}\dot{Q}_{th} - E_{el}\dot{W}_{el}} \tag{17}$$

$$CA' = \frac{\dot{m}_{CO_2,\ capt.}}{E_{NG}\dot{m}_{NG} LHV_{NG} - E_{el}\dot{W}_{el}} \tag{18}$$

$$SPECCA = \frac{\frac{1}{\eta_{H_2,eq}} - \frac{1}{\eta_{H_2,eq\ ref}}}{E_{CO_2,eq,ref} - E_{CO_2,eq}} \tag{19}$$

$$SPECCA' = \frac{\frac{1}{\eta'_{H_2,eq}} - \frac{1}{\eta'_{H_2,eq\ ref}}}{E'_{CO_2,eq,ref} - E'_{CO_2,eq}}. \tag{20}$$

The benchmark for unabated power production with and without CO_2 capture is taken from [42], i.e., advanced combined cycle configurations using H-class GTs. When steam production is considered as a valuable output, a conventional boiler and an associated emissions intensity is taken into account, as detailed in Table A5 in Appendix A, in order to determine equivalent natural gas flow and emissions.

3. Results

In this section, the process simulation results for each plant design are shown, attending to the key performance indicators defined in Section 2.3. Results of the SMR benchmark plants, the GSR and GSPOX designed for H_2 production only and the GSPOX hybrid concept with H_2 and electricity co-production, are provided, using the unabated NGCC

efficiency and CO_2 intensity as reference electricity production plant. The effect of CO_2 capture integration in the reference electricity plant is presented in a subsequent section. A detailed summary of the results from each process model is shown in the Plant Results Summary in the Appendix .

3.1. Plant Model Results

The efficiency results and CO_2 capture performance of the benchmark SMR plants without CO_2 abatement and with CO_2 capture employing MDEA absorption, as well as the GSR and GSPOX H_2 production plants and the GSPOX H_2-power co-production schemes, are shown in Figure 12. Efficiency results are indicated attending to the definitions presented in Section 2.3. It can be seen that when steam exports are neglected in the calculation, the equivalent efficiency reduction is greatest for the unabated SMR plant, while it remains unchanged for the GSPOX H_2-power plants (since there are no steam exports).

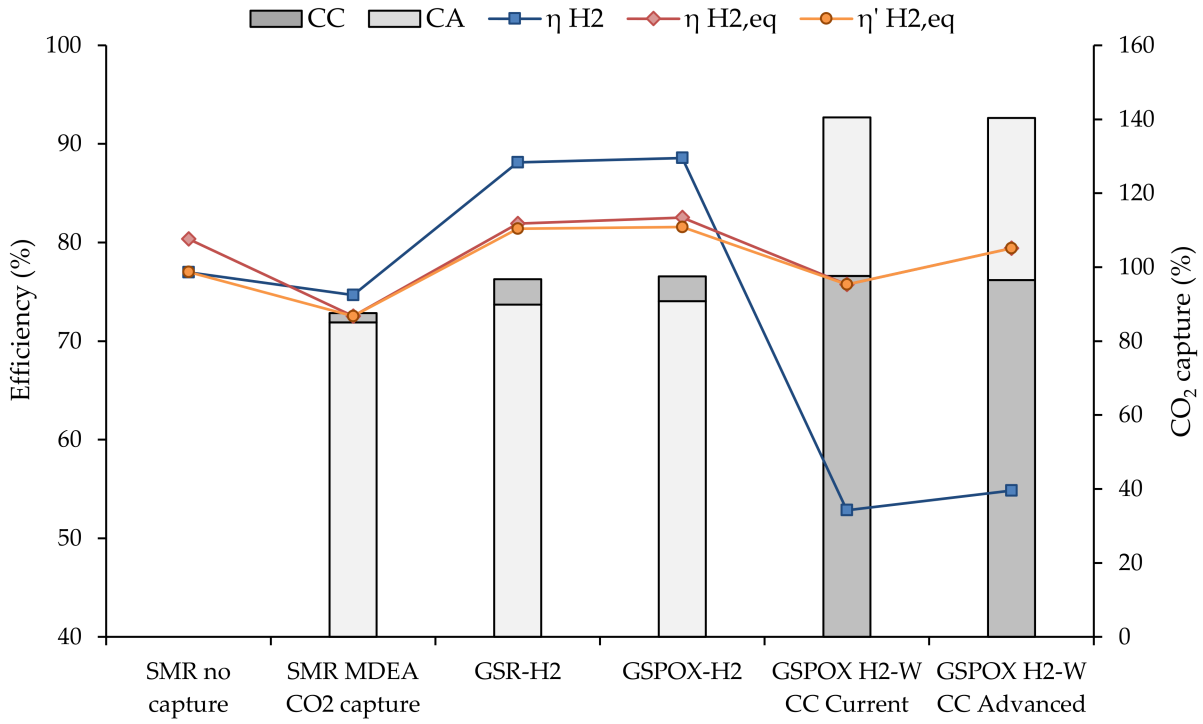

Figure 12. Efficiency and CO_2 capture results for the different cases.

The equivalent efficiency penalty for CO_2 capture with MDEA absorption amounts to approximately 7.9%-points (when accounting for steam exports). As discussed, this penalty originates from the fact that a fraction of the H_2 produced must be invested to provide heat to the reformer. Since the operation is carried out with a high S/C ratio of 4, the steam turbine low-pressure stage output is comparatively reduced. Furthermore, LP steam must be sent to the MDEA stripper reboiler for solvent regeneration, neglecting the efficiency benefit of steam export attained in the unabated SMR plant. When the energy from exported steam is neglected as a useful by-product, the energy penalty of the MDEA process reduces to only 4.5%-points: the LP steam produced is fully utilized for solvent regeneration in the CO_2 stripper reboiler. Simulation results in this work yield a significantly higher hydrogen efficiency for the SMR with MDEA capture process relative to what has been presented by Spallina et al. [11]. Reformer inlet and outlet conditions are identical, yet apparently, the fuel demand to satisfy the reformer balance is notably smaller, yielding a higher H_2 output. Equivalent efficiency on the other hand is close to the value reported by Martínez et al. [43], albeit the fact that in the present work no LP steam exports are considered for this model and the H_2 is compressed to 150 bar. Given

the higher steam turbine output in these works, it is concluded that in these earlier works a larger portion of the final H_2 product is combusted to generate more steam for the turbine in the reformer heat recovery network in order to minimize electricity imports to the plant, therefore attaining a comparatively lower amount of H_2 product. Since the GS-based plants are modeled assuming substantial electricity imports, the SMR model with MDEA CO_2 capture is designed to generate only sufficient steam for the reformer and stripper column demands.

Regarding the GS-based plants, as predicted by Nazir et al. [22], the integration of GS clusters for H_2 production results in a substantial increase (in this work up to 11.6%-points) of the H_2 efficiency relative to conventional SMR. As discussed earlier, this is a consequence of the higher reforming temperature that shifts the SMR reaction to the products side (consequently reducing the S/C ratio), as well as a more effective heat recovery network, minimizing the heat losses in the plant. On the other hand, for the GS plants with electricity imports (cases GSR-H_2 and GSPOX-H_2), similar results are obtained for the plants operating at a reactor pressure of 32.7 bar. Approximately the same amount of steam must be raised for the GSPOX prior to the WGS unit, leading to a similar H_2 production (around 0.5%-points higher for the GSPOX).

A sensitivity study regarding the cluster operating pressure is carried out and shown in Figure 13, to assess the effect on the efficiency of the reduced equilibrium conversion resulting from higher pressures in the GSR process. In this sensitivity study, it was assumed, in order not to distort the efficiency trends, that all turbomachinery components (air and PSA off-gas compressors) operate in a single adiabatic stage.

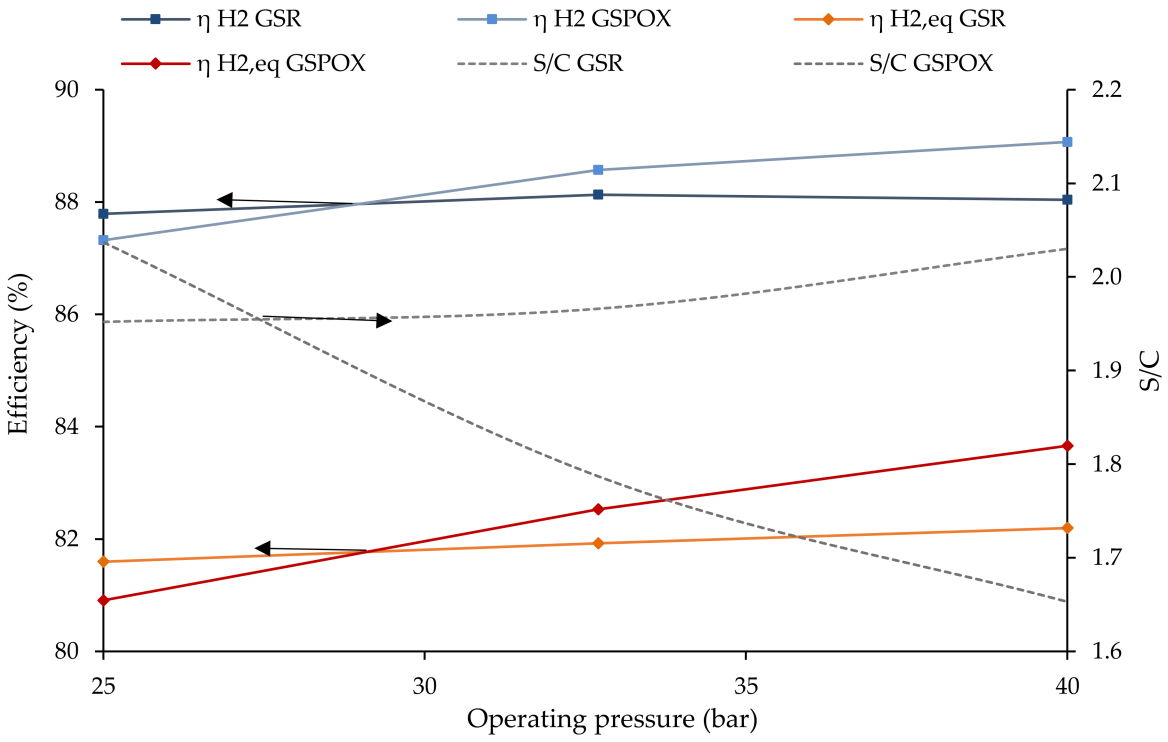

Figure 13. Effect of reactor operating pressure for GSR and GSPOX H_2 plants.

Mild benefits are reached with the GSPOX configuration: The S/C clearly declines for higher pressures, as it is not required to convert as much CO in the shift units due to the higher recovery of H_2 in the PSA, leading to better heat recuperation of the streams fed to the cluster and increased H_2 efficiency. More low-grade heat is converted to steam, resulting in a consistent improvement of the equivalent efficiency, as shown in Figure 13. For the GSR, higher pressures increase the required S/C to reach the desired methane conversion in the cluster, and consequently, the H_2 efficiency is curtailed. It is concluded

that if the turbomachinery can reach the specified pressures cost-effectively (or alternatively adding intercooled stages), the GSPOX carrier will only result in small benefits relative to the GSR. However, this advantage can be expected to continue increasing for even higher pressures, although practical challenges will constrain the maximum achievable system pressure. If, for instance, higher pressure ratios are attained by means of intercooled compression, the lower air temperature entering the oxidation step will result in lower H_2 efficiencies relative to the single adiabatic compression mode of operation because more fuel is combusted to reach the desired reactor temperature. Simultaneously, higher pressures will reduce the number of H_2 and CO_2 compression stages required to reach delivery pressures, reducing the capital costs of these items. Thus, this parameter is closely interlinked with the remaining plant elements. However, it should also be noted that higher operating pressures in the reactor increase undesired mixing of the outlet streams from the different steps of the reactor cycle, reducing the CO_2 avoidance. In the range of pressures studied here, the CO_2 avoidance was reduced by 1.0 and 1.5%-points for GSR and GSPOX plants when increasing the pressure from 25 to 40 bar.

As the advantages of GSPOX over GSR for H_2 production are relatively small, the present assessment is extended by integrating a combined power cycle with the GSPOX to simultaneously produce H_2 and power. The key operational feature from the GSPOX that allows this with reduced energy penalty is the possibility of producing a relatively pure H_2 stream which can be used for extra firing if the air is introduced in the cluster with an excess of O_2. As expected, the Advanced GT combined cycle configuration yields the most attractive results, approximately 3.4%-points of additional equivalent efficiency points compared to the model employing Current GT technology. Still, the equivalent efficiency is around 1.0%-points below the unabated SMR benchmark. Given the pressure ratio of each GT, the H_2 recovery and consequently the H_2 efficiency vary slightly. Indeed, the H_2 recovery drops in the PSA unit at lower inlet pressure, falling from 85.6% to 82.0%, when shifting from Advanced to Current GT technology.

For the GSPOX power generating plants, given the fixed natural gas input of 129 MW (LHV basis), the net electricity production resulted in around 25 MW as shown in Figure 14 (~20% of the heat input) whereas the H_2 output (LHV basis) decreased by approximately 30% relative to the unabated SMR process. An effective operational handle to trade-off H_2 production for additional electricity would be to operate the PSA with a higher off-gas desorption pressure (such that the size of the associated compression unit is reduced), but this is limited to the extent that H_2 production in water splitting step of the GSPOX is sufficient to reach COT GT values in the extra firing chamber (unless the H_2 product is also employed for extra firing, which would imply additional penalties and process variations). Heat rejected comparatively increases relative to the SMR H_2 production plant without CO_2 capture due to the inherent thermodynamic inefficiencies related to a larger fuel degradation for power generation, reaching a degree of overall losses comparable to the SMR MDEA capture process. The effective use of low-grade heat across the plant in the H_2-power configurations for additional electricity production prevents the need to export any LP steam. Interestingly, both GSPOX H_2-power plants deliver a similar electricity output, underlying the higher efficiency of the Advanced GT power production scheme, which accomplishes the same amount of electricity production with a lower fraction of the heating value (given the fact that the H_2 production is somewhat higher due to the increased recovery in the PSA).

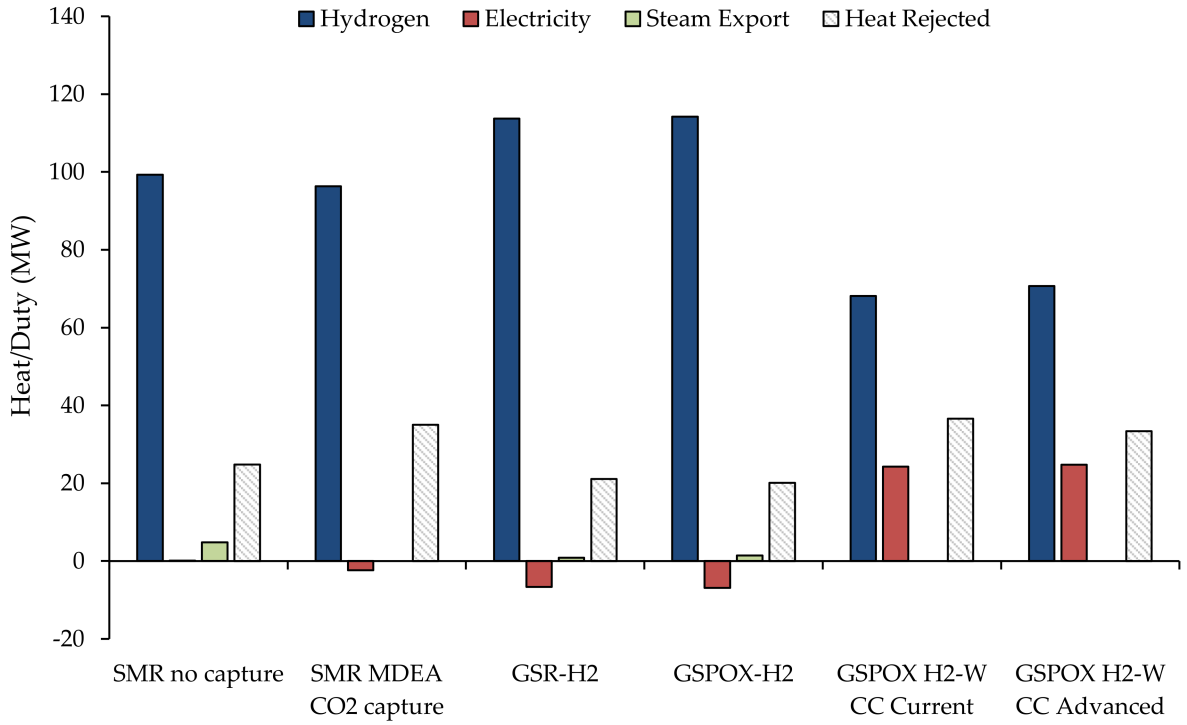

Figure 14. Power-energy breakdown for the different plants.

Scale is another important consideration in such combined power and hydrogen plants. The plant with Advanced GT technology will need to be very large (around 20× the heat input of the plants presented in this work), given the size of the heavy-duty gas turbines required to maximize firing temperature and efficiency. Such plants can only be considered for the longer-term future when a large hydrogen market has been established. Efficiencies representative of the Current GT technology can be achieved by much smaller industrial gas turbines [55], only requiring an increase in plant size of ~3×. Such a plant could supply an industrial cluster with power and hydrogen, avoiding any dependency on a broader integrated hydrogen market.

For the GSR and GSPOX H_2 plants, a small export of LP steam is needed in both cases. Furthermore, electricity imports of approximately 5% of the natural gas heat input are required. However, the heat rejected is reduced to around 16% of the heat input, in effect around 4%-points and 11%-points below the unabated SMR plant and SMR plant with MDEA CO_2 capture, respectively.

In terms of emissions, MDEA absorption integration achieves a CO_2 avoidance of approximately 85% (Figure 12), similar to earlier published works. CO_2 emissions are not curtailed entirely due to a small remaining fraction of CO, CH_4 and CO_2 present in the PSA off-gas used as fuel in the reformer. The CO_2 avoidance for the GSR and GSPOX is approximately 5%-points above the MDEA benchmark, due to the large capture rate (>95%) achieved with inherent CO_2 capture in the GS concepts. However, CO_2 avoidance is considerably less than the CO_2 capture rate due to the associated emissions resulting from the imported electricity generation. On the other hand, for the H_2-power co-generating concepts, since electricity is produced with inherent CO_2 capture, the CO_2 avoidance is largely above the capture ratio, reaching values above 140%.

In terms of equivalent specific emissions, reflected in Figure 15, the value decreases for the SMR plant without capture due to a small export of steam (and associated CO_2 avoidance of a boiler), whereas for the plant with MDEA capture it increases, due to the associated emissions of electricity imports. A similar trend is seen for the GSR and GSPOX H_2 production plants. For the concepts that produce additional electricity with CO_2 capture, the equivalent specific emissions become negative. Finally, regarding the

SPECCA indexes, it can be seen that the value obtained with the SMR with MDEA CO_2 capture benchmark is substantially reduced when implementing GS-based CO_2 capture in the remaining models. In fact, when the efficiency of a specific plant is above the reference unabated SMR benchmark, the SPECCA index turns out to be negative. Indeed, this is a consequence of a negative energy penalty when integrating inherent CO_2 capture technology. If the SPECCA index is evaluated using equivalent efficiency values which do not account for the steam exports as a beneficial outcome from the plant (both for the specific plant with CO_2 capture and the reference plant), the SPECCA index becomes even smaller, as the associated CO_2 intensive steam generation in boilers is not considered.

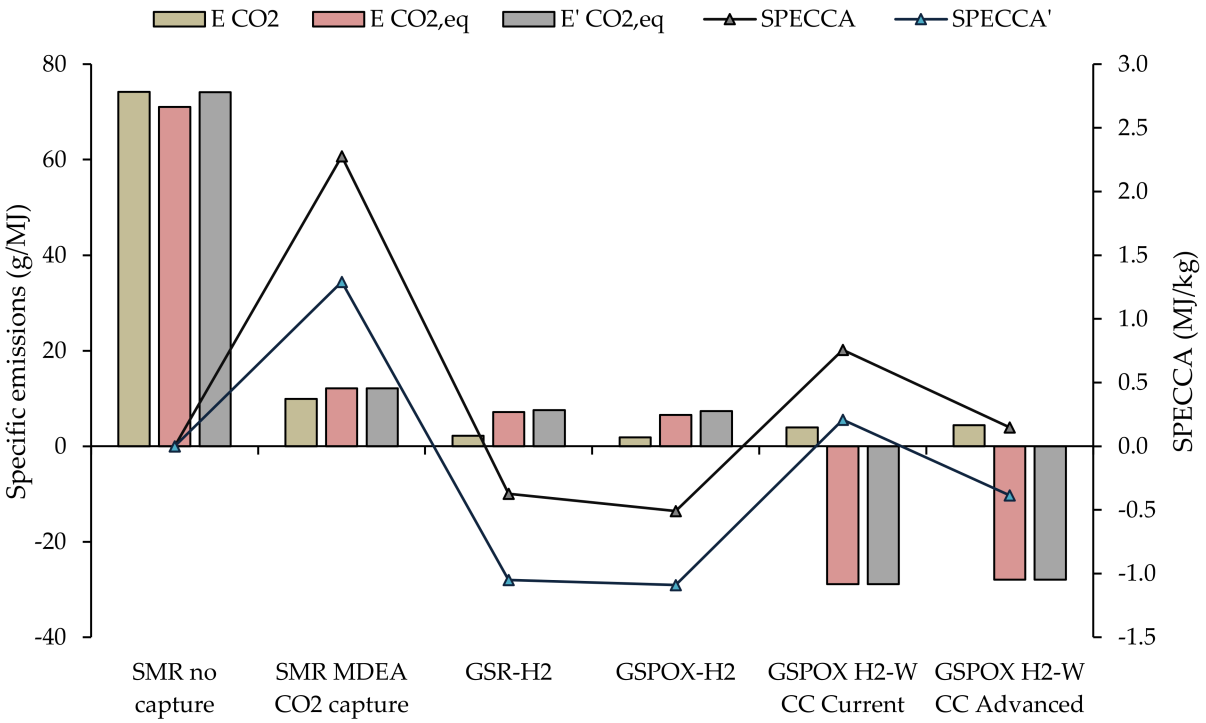

Figure 15. Specific emissions and SPECCA indexes for the different plants.

Lastly, it should be noted that due to the substantial mixing occurring in the GS clusters, the purity of the CO_2 stream obtained after cooling and water knockout resulted in >90 mol% of CO_2. It was assumed that the larger proportion of impurities (primarily N_2) was acceptable for transport and storage conditions and that a higher compression duty resulting from these lower boiling point gases was considered acceptable. However, some sources recommend CO_2 purities >96 mol%, for which a purification unit may be required [56]. The overall power consumption will be minimally affected, with a marginal increase of specific emissions (due to purging in the purification unit), although the addition of cryogenic exchangers and vessels will lead to a higher overall plant cost [57].

3.2. Effect of Electricity Utilities

The critical parameter affecting the equivalent efficiency and emissions performance of the novel GSPOX plants presented in this study is the efficiency and CO_2 emissions intensity of the reference power plants. As explained at the beginning of the Results section, the results presented earlier are determined considering an efficient NGCC power plant using H-class GTs without CO_2 capture as a reference electricity generation plant (a completely unabated value chain). In this section, the previous results are compared to the case where electricity production with CO_2 capture is used as a reference plant, using the performance values shown in Table A5 in Appendix A.

It is noted that the calculations reflected in this section account for steam exports. Similar effects as shown in the previous section would be observed if steam exports are neglected. Given the negligible electricity production in the unabated SMR plant, sensitivity to the electricity utilities is not presented for this case.

Figure 16 shows the equivalent efficiency (left axis) and CO_2 avoidance (right axis) for each model. When considering electricity generation with CO_2 capture, the equivalent H_2 production efficiency of the plants that import electricity decreases, whereas the plants exporting electricity benefit from a less efficient reference.

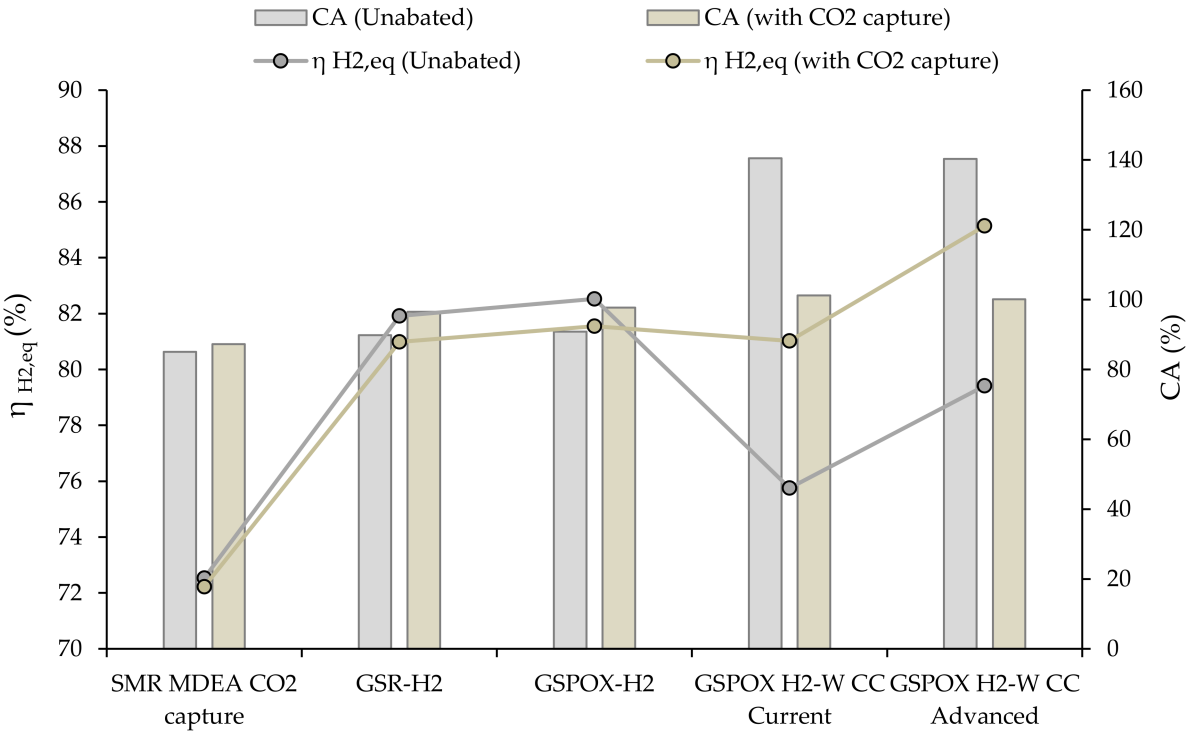

Figure 16. H_2 equivalent efficiencies and CO_2 avoidance of the H_2-power production concepts for electricity generation reference plants with and without CO_2 capture.

On the other hand, when looking at the CO_2 avoidance, this parameter slightly increases for the importing electricity plants (H_2 production), when it is provided by a power plant with CO_2 capture. On the other hand, the CO_2 avoidance of the GSPOX CC plants decreases to around 100% because low-carbon electricity exports now displace electricity from a low-carbon reference plant. This is further emphasized in the equivalent CO_2 emissions values shown in Figure 17: For reference electricity generation with CO_2 capture, they slightly decrease for power importing plants, while in the H_2-power co-production schemes they increase from an originally negative value to slightly above zero.

The influence in the SPECCA index of these combined effects is also reflected in Figure 17. For the SMR plant with MDEA CO_2 capture, very small variations are observed, given the overall small electricity imports that result in very similar equivalent efficiencies. For the H_2 producing plants, electricity imports with CO_2 capture tend to increase the SPECCA index (mainly due to the lower equivalent H_2 efficiency). For the power-producing GSPOX plants, the large increase in equivalent H_2 efficiency (due to a less efficient reference electricity production with CO_2 capture) leads to negative SPECCA values in both cases.

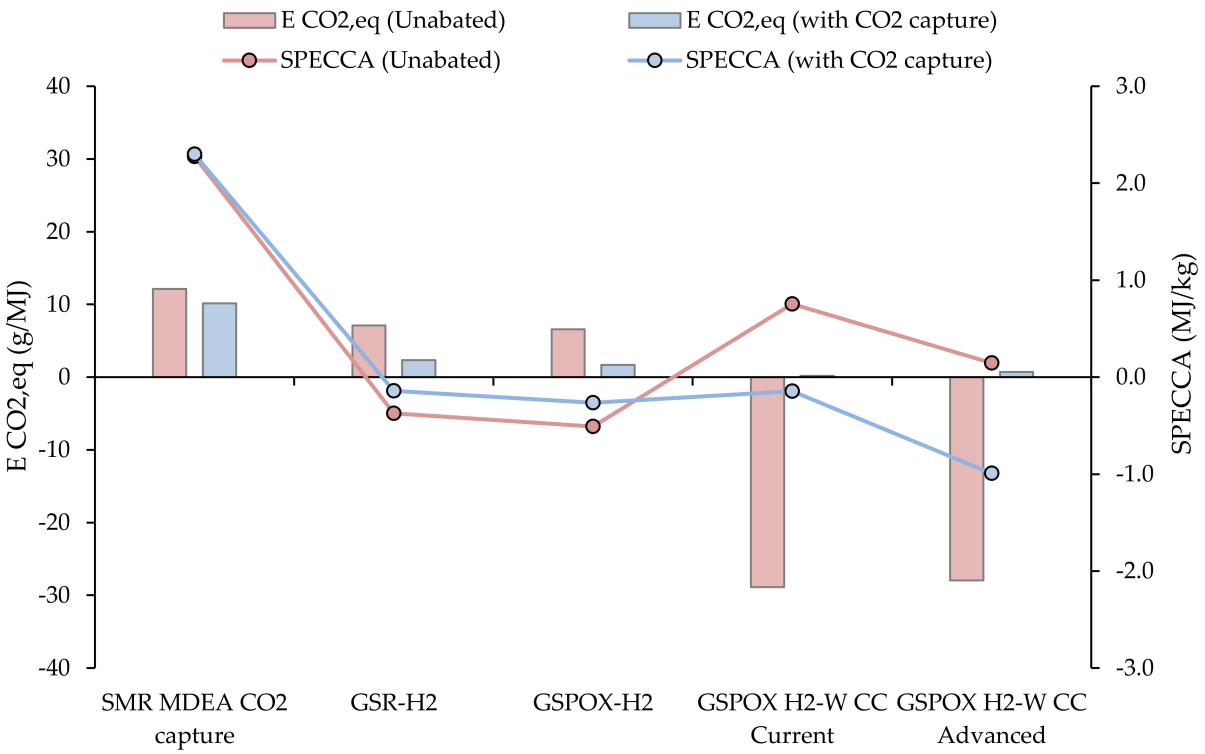

Figure 17. Equivalent CO_2 emissions and SPECCA indexes of the H_2-power production processes for electricity generation reference plants with and without CO_2 capture.

4. Summary and Conclusions

This study investigated the potential of a novel La-Fe-based oxygen carrier with thermodynamic properties that enable the partial oxidation of natural gas with integrated CO_2 capture. Such an oxygen carrier can avoid the equilibrium limitations restricting conventional catalytic methane reforming and facilitates direct hydrogen production via the water-splitting reaction. In addition, it can alleviate safety concerns related to the toxicity of Ni-based reforming catalysts. The benefits facilitated by these features were quantified and compared to three benchmarks: conventional steam methane reforming (SMR), SMR with conventional CO_2 capture (pre-combustion MDEA absorption), and the gas switching reforming (GSR) process using a Ni-based oxygen carrier.

In terms of equivalent H_2 production efficiencies, it was shown that the novel gas switching partial oxidization (GSPOX) process achieved mild benefits relative to the GSR concept (of around 0.6%-points for the case with reactor operating pressure of 32.7 bar). Even though GSPOX could convert methane with a much lower steam requirement, a similar amount of steam as in GSR is needed in the subsequent water-gas shift reactors to maximize hydrogen production. Next, the possibility of designing the GSPOX plant for H_2 and power co-production was investigated. A semi-pure H_2 fuel stream can be produced for extra firing; to heat the depleted air stream from the GSPOX oxidation step outlet temperature to the gas turbine firing temperature for high-efficiency power production. Thus, the cluster was integrated into combined power cycles with two different firing temperatures, representative of two GT technology levels. In terms of equivalent H_2 efficiencies, the Current and Advanced GT configurations were 4.5 and 0.9%-points below the unabated SMR benchmark, respectively, but both plants achieved equivalent CO_2 avoidance of 140% because of considerable low-carbon electricity exports. When an NGCC plant with CO_2 capture was taken as reference for imported/exported electricity, CO_2 avoidance was approximately 100% with equivalent H_2 production efficiencies 0.7 and 4.8%-points higher than the SMR benchmark.

In comparison to the GSR technology with Ni-based oxygen carriers, the GSPOX process in H_2 mode shows mild improvements that increase with pressure. When operated at 40 bar, the GSPOX-H_2 plant achieves 1.5%-points higher equivalent H_2 production efficiency than GSR with similar CO_2 avoidance. The combined power and H_2 GSPOX configuration with the Advanced gas turbine can increase this benefit to 4.1%-points when exported electricity is assumed to displace NGCC power production with CO_2 capture. However, such an efficient power cycle requires a large gas turbine that will lead to a plant with a very high hydrogen output, which will only be feasible when a large hydrogen market is established. When a smaller and less efficient gas turbine is used, the GSPOX co-production plant offers no efficiency benefits relative to GSR. However, such a smaller plant will be a good option for independent clean power and hydrogen supply to an industrial cluster.

To conclude, the successful development of a GSPOX oxygen carrier can further increase the efficiency gains promised by GSR, producing clean "blue" hydrogen at a higher efficiency than carbon-intensive "grey" hydrogen from steam methane reforming. These gains increase when the system can be operated at very high pressures or market conditions allow for the construction of large, combined power and hydrogen plants. When factoring in the avoidance of toxicity concerns related to Ni-based oxygen carriers needed in GSR to catalyze the reforming reaction, further development of these novel oxygen carriers can be safely recommended.

Author Contributions: Conceptualization, S.C.; Investigation, C.A.d.P.; Formal Analysis, C.A.d.P., S.C.; Methodology, C.A.d.P., S.C.; Software C.A.d.P., A.J.A.; Writing—original draft, C.A.d.P., S.C., A.J.A., F.D.; Writing—review & editing, C.A.d.P., F.D.; Supervision, A.J.A., S.A.; Funding Acquisition, A.J.A., S.A.; Validation, F.D.; Project Administration, S.A. All authors have read and agreed to the published version of the manuscript.

Funding: This research received financial support from the ERA-NET cofund, ACT GaSTech Project number 276321 co-funded by the European Commission under the Horizon 2020 program, and ACT Grant Agreement No. 691712. The partners collaborating in this article have received funding from Ministerio de Economía y Competitividad (MINECO), Spain (reference PCIN-2017-013), the Research Council of Norway, Norway, and the Swiss Federal Office of Energy, Switzerland.

Institutional Review Board Statement: Not applicable.

Informed Consent Statement: Not applicable.

Data Availability Statement: Not applicable.

Acknowledgments: The authors would like to acknowledge Honeywell for the free Academic License of Unisim Design Suite R451 and AmsterChem for the Academic CAPE-OPENicense.

Conflicts of Interest: The authors declare no conflict of interest.

Abbreviations

CA	CO_2 Avoided
CC	CO_2 Captured
CCS	Carbon Capture and Storage
Ch	Chargeable
CLC	Chemical Looping Combustion
CLR	Chemical Looping Reforming
CSTR	Continuous Stirred Tank Reactor
FTR	Fired Tubular Reformer
COT	Combustor Outlet Temperature
GHG	Greenhouse Gases
GSPOX	Gas Switching Partial Oxidation
GS	Gas Switching
GSR	Gas Switching Reforming

GT	Gas Turbine
HTS	High Temperature Shift
IEA	International Energy Agency
IPCC	Intergovernmental Panel on Climate Change
LHV	Lower Heating Value
LP	Low Pressure
LT	Low Temperature
LTS	Low Temperature Shift
MDEA	Methyl-Diethanolamine
MEA	Methyl-Ethanolamine
nCh	Non-chargeable
NG	Natural Gas
NGCC	Natural Gas Combined Cycle
POX	Partial Oxidation
PSA	Pressure Swing Adsorption
RED	Reduction
REF	Reforming
TIT	Turbine Inlet Temperature
TOT	Turbine Outlet Temperature
SMR	Steam Methane Reforming
SPECCA	Specific Primary Energy Consumption for CO_2 Avoided.
S/C	Steam to Carbon
WGS	Water Gas Shift
WS	Water Splitting
Symbols	
b	Cooling constant
c_p	Specific heat capacity (J/mol·K)
h	Specific enthalpy (J/mol)
n	Total moles (mol)
F	Total flow (mol/s)
K	Equilibrium constant (-)
k	Pressure drop constant (-)
P	Pressure (bar)
p	Partial pressure (bar)
r	Species reaction rate (mol/s)
R	Gas Constant (J/molK)
R_{H_2}	Hydrogen recovery (%)
s	Selectivity (%)
t	Time (s)
T	Temperature (K)
y	Molar fraction in gas (-)
ξ	Global reaction rate (mol/s)
φ	Coolant–got gas mass flow fraction
$\Delta H_{r,T}$	Enthalpy of reaction (kJ/mol)
Subscripts and Superscripts	
k	Component
i	Stream
r	Reaction/Rotor
^{o}	Ambient/reference conditions
-	Averaged value
s	Stator
g	Gas
bl	Blade
des	Desorption
ads	Adsorption

Appendix A

Appendix A.1. Modeling Assumptions

Table A1. H2 plants modeling assumptions.

Item	Value	Unit
Fired tubular reformer (FTR)		
Reforming temperature	890	°C
Furnace gases temperature	1010	°C
Excess air	15	%
Air blower polytropic efficiency	80	%
Heat exchange		
Temperature approach gas-gas	30	°C
Temperature approach steam-gas	20	°C
Temperature approach liquid-gas	10	°C
Temperature approach liquid-liquid	5	°C
Air side pressure drop	5	kPa
NG/syngas/reduction gases side pressure drop	20	kPa
Turbomachinery		
Air compressor polytropic efficiency	92.5	%
Steam turbine efficiency (SMR)	80.0	%
N_2 turbine polytropic efficiency	87.0	%
CO_2 compression stage polytropic efficiency	80.0	%
H_2 compression booster/stage polytropic efficiency	80.0	%
Intercooler pressure drop	20	kPa
Other assumptions		
H_2 delivery pressure	150	bar
CO_2 delivery pressure	150	bar
Process streams cooled to	25	°C
LP steam conditions (sat.)	6	bar

Table A2. GS cluster modeling assumptions.

Item	Value	Unit
Maximum reactor temperature	1100	°C
Pressure drop	50	kPa
Thermal mass volume fraction	0.25	-
GSPOX Oxygen Carrier		
XO molecular weight	233.6	g/mol
X molecular weight	212.0	g/mol
Density (constant)	2000	kg/m^3
Inert materiel content (Al_2O_3)	20–40	wt.%

Table A3. Gas turbine modeling assumptions.

Reference Values			
Item	**F-Class (Current)**	**H-Class (Advanced)**	**Unit**
COT	1440	1648	°C
TIT	1360	1550	°C
TOT	603	640.1	°C
Pressure ratio	18.1	23.7	-
Simple cycle efficiency	39.0	43.0	%
NG-fired rated power	280.0	520.0	MW
Calibrated Parameters *			
Item	F-class (Current)	H-class (Advanced)	Unit
Compressor polytropic efficiency	92.5	94.0	%
Expander polytropic efficiency	87.0	88.0	%
Stator cooling constant b_s	0.0616	0.0534	-
Rotor cooling constant b_r	0.0674	0.0791	-
Other Parameters			
Item	F-class (Current)	H-class (Advanced)	Unit
Air filter pressure loss	1	1	%
Combustor pressure drop	3	3	%
Exhaust pressure loss (simple cycle)	1	1	kPa
Electromechanical efficiency	98.6	98.6	%
pressure drop constant k	0.07	0.07	-
Max. stator blade temperature	850	900	°C
Max. rotor blade temperature	825	875	°C

Air at 15 °C and 60% relative humidity is used for the calibration *.

Table A4. Steam cycle modelling assumptions.

Item	Value	Units
Condenser pressure	0.04	bar
Auxiliaries for heat rejection	0.008	kW/kW_{th}
Water pumps isentropic efficiency	80	%
LP/IP Pinch point	10	°C
LP/IP Approach point	9	°C
LP ΔP/P eco+eva	25	%
IP ΔP/P eco+eva	15	%
ΔP/P superheaters	8	%
HP pinch (once through)	9	°C
Exhaust air side pressure drop	3	kPa
Pressure level in drum/eva (HP/IP/LP)	185/43/6	bar
LP superheat	300	°C
LP Stage isentropic efficiency	87.7	%
IP Stage isentropic efficiency	92.0	%
HP Stage isentropic efficiency	90.3	%
Electromechanical Efficiency	98.3	%
Maximum steam temperature	565/600	°C

Appendix A.2. Modeling of Technological Components

1. PSA unit H_2 recovery correlation:

$$R_{H_2} = 100 - \frac{100}{0.251\left(\frac{P_{des}}{P_{ads}}\right) + 1.2706} \quad \text{(A1)}$$

where:
R_{H_2} is the H_2 recovery in %, assumed 100% pure H_2.

P_{ads} is the inlets syngas pressure in a bar at which adsorption of non-H_2 components takes place.
P_{ads} is the regeneration bed desorption pressure in a bar of the PSA off-gas.

2. Gas Turbine units:

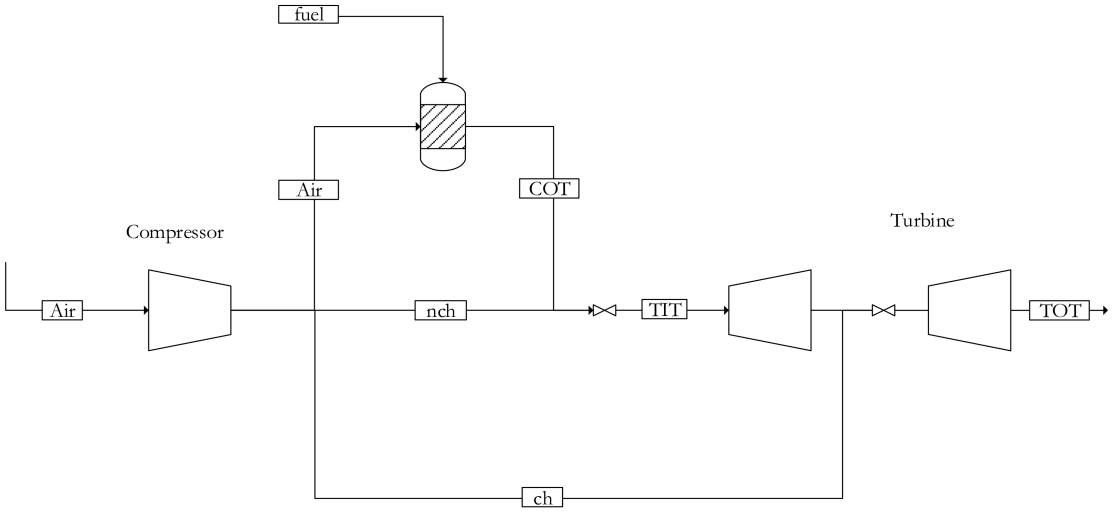

Figure A1. Simplified gas turbine model with cooling flows.

Stator (s) and Rotor (r) coolant flow fraction calculation:

$$\frac{\dot{m}_s \bar{c}_{p,s}}{\dot{m}_g \bar{c}_{p,g}} = b_s \frac{\left(T_{g,i} - T_{bl,s}\right)}{\left(T_{bl,s} - T_{s,i}\right)} \tag{A2}$$

$$\frac{\dot{m}_r \bar{c}_{p,r}}{\dot{m}_g \bar{c}_{p,g}} = b_r \frac{\left(T_{g,i} - T_{bl,r}\right)}{\left(T_{bl,r} - T_{r,i}\right)}. \tag{A3}$$

Pressure drop for coolant and hot gas path mixing flows:

$$\frac{\Delta p}{p} = k\varphi. \tag{A4}$$

Appendix A.3. Reference Plant Efficiency and CO_2 Intensity

Table A5. Efficiency and emissions intensity for natural gas and reference steam and electricity plants.

Plant Product/Feed	Efficiency (%)	CO_2 Emissions Intensity ($kgCO_2/MJ$)
Electricity (Unabated)	62.1	0.0923
Electricity (with CO_2 capture)	54.0	0.0106
Steam	90.0	0.0633
Natural gas	-	0.0568

Appendix A.4. Plant Results Summary

Table A6. Plant Results Summary.

Product	**H_2 and Steam**				**H_2 and Power**	
Reformer	FTR	FTR	GSR	GSPOX	GSPOX	GSPOX
Topping cycle	None	None	LT air GT	LT air GT	Current GT	Advanced GT
Bottoming cycle	Steam turbine	Steam turbine	Boilers	Boilers	Steam Cycle	Steam Cycle
Model	SMR no capture	SMR MDEA CO_2 capture	GSR-H_2	GSPOX-H_2	GSPOX H_2-W CC Current	GSPOX H_2-W CC Advanced
Operating Parameters						
COT	-	-	1042	992	1441	1648
TIT	-	-	1042	992	1361	1550
Reactor Pressure (bar)	32.7	32.7	32.7	32.7	18.34	23.91
Overall S/C	2.70	4.00	1.97	1.79	0.91	1.05
$m_{eq.\ NG}$ (kg/s)	2.66	2.86	2.98	2.977	1.93	1.92
$m'_{eq.\ NG}$ (kg/s)	2.77	2.86	3.00	3.01	1.93	1.92
H_2 production (kg/s)	0.827	0.80	0.95	0.95	0.57	0.59
Efficiencies						
$\eta\ H_2$ (%)	76.97	74.66	88.13	88.57	52.84	54.83
$\eta\ H_{2.eq}$ (%)	80.35	72.53	81.92	82.53	75.76	79.42
$\eta'\ H_{2.eq}$ (%)	77.00	72.53	81.39	81.58	75.76	79.42
Power breakdown						
Air compressor/blower (MW)	0.68	0.71	6.60	6.50	-	-
H_2 compressor (MW)	2.27	2.26	2.65	2.66	2.22	1.97
Off-gas compressor (MW)	0.00	0.00	4.29	4.29	2.82	3.00
CO_2 compressor (MW)	0.00	2.08	0.61	0.64	1.01	0.86
Steam turbine net (MW)	3.12	3.04	-	-	10.87	9.76
Gas turbine net/N_2 turbine (MW)	0.00	0.00	7.54	7.25	20.92	21.13
Pumps and other aux. (MW)	0.13	0.32	0.03	0.03	0.31	0.25
Net electricity (MW)	0.04	−2.35	−6.64	−6.87	24.23	24.80
Steam export (MW)	4.83	0.00	0.82	1.45	0.00	0.00

Table A6. *Cont.*

Product		**H_2 and Steam**			**H_2 and Power**	
Emissions Performance						
E_{CO2} (g/MJ)	74.18	9.90	2.19	1.83	3.94	4.41
$E_{CO2.eq}$ (g/MJ)	71.06	12.14	7.12	6.57	−28.87	−27.95
$E'_{CO2.eq}$ (g/MJ)	74.14	12.14	7.58	7.38	−28.87	−27.95
CC (%)	0.00	87.57	96.74	97.51	97.62	96.51
CA (%)	-	85.06	89.86	90.80	140.50	140.36
CA′ (%)	-	85.06	89.28	89.75	140.50	140.36
SPECCA (MJ/kg)	-	2.28	−0.37	−0.51	0.76	0.15
SPECCA′ (MJ/kg)	-	1.29	−1.05	−1.09	0.21	−0.39

References

1. Masson-Delmotte, V.; Zhai, P.; Pörtner, H.; Roberts, D.; Skea, J.; Shukla, P.R.; Pirani, A.; Moufouma-Okia, W.; Péan, C.; Pidcock, R. Global Warming of 1.5 OC: An IPCC Special Report on the Impacts of Global Warming of 1.5 °C Above Pre-industrial Levels and Related Global Greenhouse Gas Emission Pathways, in the Context of Strengthening the Global Response to the Threat of Climate Change, Sustainable Development, and Efforts to Eradicate Poverty. Available online: https://www.ipcc.ch/sr15/ (accessed on 20 May 2021).
2. Anonymous. *The Future of Hydrogen*; IEA: Paris, France, 2019.
3. Voldsund, M.; Jordal, K.; Anantharaman, R. Hydrogen production with CO_2 capture. *Int. J. Hydrogen Energy* **2016**, *41*, 4969–4992. [CrossRef]
4. Nazir, H.; Louis, C.; Jose, S.; Prakash, J.; Muthuswamy, N.; Buan, M.E.M.; Flox, C.; Chavan, S.; Shi, X.; Kauranen, P.; et al. Is the H2 economy realizable in the foreseeable future? Part I: H2 production methods. *Int. J. Hydrogen Energy* **2020**, *45*, 13777–13788. [CrossRef]
5. Nazir, H.; Muthuswamy, N.; Louis, C.; Jose, S.; Prakash, J.; Buan, M.E.M.; Flox, C.; Chavan, S.; Shi, X.; Kauranen, P.; et al. Is the H2 economy realizable in the foreseeable future? Part III: H2 usage technologies, applications, and challenges and opportunities. *Int. J. Hydrogen Energy* **2020**, *45*, 28217–28239. [CrossRef] [PubMed]
6. Parra, D.; Valverde, L.; Pino, F.J.; Patel, M.K. A review on the role, cost and value of hydrogen energy systems for deep decarbonisation. *Renew. Sustain. Energy Rev.* **2019**, *101*, 279–294. [CrossRef]
7. Schnuelle, C.; Wassermann, T.; Fuhrlaender, D.; Zondervan, E. Dynamic hydrogen production from PV & wind direct electricity supply–Modeling and techno-economic assessment. *Int. J. Hydrogen Energy* **2020**, *45*, 29938–29952.
8. Gardarsdottir, S.O.; Voldsund, M.; Roussanaly, S. Comparative Techno-Economic Assessment of Low CO_2 Hydrogen Production Technologies. Available online: https://www.sintef.no/globalassets/project/hyper/presentations-day-1/day1_1200_gardarsdottir_comparative-techno-economic-assessment-of-low-co2-hydrogen-production-technologies_sintef.pdf (accessed on 20 May 2021).
9. Cloete, S.; Ruhnau, O.; Hirth, L. On capital utilization in the hydrogen economy: The quest to minimize idle capacity in renewables-rich energy systems. *Int. J. Hydrogen Energy* **2020**, *46*, 169–188. [CrossRef]
10. Dickel, R. *Blue Hydrogen as an Enabler of Green Hydrogen: The Case of Germany*; The Oxford Institute for Energy Studies: Oxford, UK, 2020. [CrossRef]
11. Spallina, V.; Pandolfo, D.; Battistella, A.; Romano, M.C.; Annaland, M.V.; Gallucci, F. Techno-economic assessment of membrane assisted fluidized bed reactors for pure H_2 production with CO_2 capture. *Energy Convers. Manag.* **2016**, *120*, 257–273. [CrossRef]
12. Cormos, A.; Szima, S.; Fogarasi, S.; Cormos, C. Economic assessments of hydrogen production processes based on natural gas reforming with carbon capture. *Chem. Eng. Trans.* **2018**, *70*, 123.
13. Miricioiu, M.G.; Iacob, C.; Nechifor, G.; Niculescu, V. High Selective Mixed Membranes Based on Mesoporous MCM-41 and MCM-41-NH2 Particles in a Polysulfone Matrix. *Front. Chem.* **2019**, *7*, 332. [CrossRef]
14. Miricioiu, M.G.; Niculescu, V.; Filote, C.; Raboaca, M.S.; Nechifor, G. Coal Fly Ash Derived Silica Nanomaterial for MMMs—Application in CO_2/CH4 Separation. *Membranes* **2021**, *11*, 78. [CrossRef]
15. Miricioiu, M.G.; Niculescu, V. Fly Ash, from Recycling to Potential Raw Material for Mesoporous Silica Synthesis. *Nanomaterials* **2020**, *10*, 474. [CrossRef]
16. Ishida, M.; Zheng, D.; Akehata, T. Evaluation of a chemical-looping-combustion power-generation system by graphic exergy analysis. *Energy* **1987**, *12*, 147–154. [CrossRef]
17. Rydén, M.; Lyngfelt, A.; Mattisson, T. Synthesis gas generation by chemical-looping reforming in a continuously operating laboratory reactor. *Fuel* **2006**, *85*, 1631–1641. [CrossRef]
18. Nazir, S.M.; Morgado, J.F.; Bolland, O.; Quinta-Ferreira, R.; Amini, S. Techno-economic assessment of chemical looping reforming of natural gas for hydrogen production and power generation with integrated CO_2 capture. *Int. J. Greenh. Gas Control.* **2018**, *78*, 7–20. [CrossRef]
19. Mattisson, T.; Keller, M.; Linderholm, C.; Moldenhauer, P.; Rydén, M.; Leion, H.; Lyngfelt, A. Chemical-looping technologies using circulating fluidized bed systems: Status of development. *Fuel Process Technol.* **2018**, *172*, 1–12. [CrossRef]
20. Zaabout, A.; Cloete, S.; Johansen, S.T.; Van, S.A.; Gallucci, F.; Amini, S. Experimental demonstration of a novel gas switching combustion reactor for power production with integrated CO_2 capture. *Ind. Eng. Chem. Res.* **2013**, *52*, 14241–14250. [CrossRef]
21. Wassie, S.A.; Gallucci, F.; Zaabout, A.; Cloete, S.; Amini, S.; van Sint Annaland, M. Hydrogen production with integrated CO_2 capture in a novel gas switching reforming reactor: Proof-of-concept. *Int. J. Hydrogen Energy* **2017**, *42*, 14367–14379. [CrossRef]
22. Nazir, S.M.; Cloete, J.H.; Cloete, S.; Amini, S. Efficient hydrogen production with CO_2 capture using gas switching reforming. *Energy* **2019**, *185*, 372–385. [CrossRef]
23. Spallina, V.; Marinello, B.; Gallucci, F.; Romano, M.C.; Van Sint Annaland, M. Chemical looping reforming in packed-bed reactors: Modelling, experimental validation and large-scale reactor design. *Fuel Process Technol.* **2017**, *156*, 156–170. [CrossRef]
24. Nazir, S.M.; Cloete, J.H.; Cloete, S.; Amini, S. Pathways to low-cost clean hydrogen production with gas switching reforming. *Int. J. Hydrogen Energy* **2020**. [CrossRef]

25. Ugwu, A.; Zaabout, A.; Tolchard, J.R.; Dahl, P.I.; Amini, S. Gas Switching Reforming for syngas production with iron-based oxygen carrier-the performance under pressurized conditions. *Int. J. Hydrogen Energy* **2020**, *45*, 1267–1282. [CrossRef]
26. Zaabout, A.; Dahl, P.I.; Ugwu, A.; Tolchard, J.R.; Cloete, S.; Amini, S. Gas Switching Reforming (GSR) for syngas production with integrated CO_2 capture using iron-based oxygen carriers. *Int. J. Greenhouse Gas Control* **2019**, *81*, 170–180. [CrossRef]
27. Kang, Y.; Tian, M.; Huang, C.; Lin, J.; Hou, B.; Pan, X.; Li, L.; Rykov, A.I.; Wang, J.; Wang, X. Improving Syngas Selectivity of Fe2O3/Al2O3 with Yttrium Modification in Chemical Looping Methane Conversion. *ACS Catal.* **2019**, *9*, 8373–8382. [CrossRef]
28. Kang, D.; Lim, H.S.; Lee, M.; Lee, J.W. Syngas production on a Ni-enhanced Fe2O3/Al2O3 oxygen carrier via chemical looping partial oxidation with dry reforming of methane. *Appl. Energy* **2018**, *211*, 174–186. [CrossRef]
29. Zhu, X.; Imtiaz, Q.; Donat, F.; Müller, C.R.; Li, F. Chemical looping beyond combustion—A perspective. *Energy Environ. Sci.* **2020**, *13*, 772–804. [CrossRef]
30. Li, D.; Xu, R.; Gu, Z.; Zhu, X.; Qing, S.; Li, K. Chemical-looping conversion of methane: A review. *Energy Technol.* **2020**, *8*, 1900925. [CrossRef]
31. Donat, F.; Müller, C.R. CO_2-free conversion of CH4 to syngas using chemical looping. *Appl. Catal. B Environ.* **2020**, *278*, 119328. [CrossRef]
32. Robie, R.A.; Hemingway, B.S. *Thermodynamic Properties of Minerals and Related Substances at 298.15 K and 1 bar (105 Pascals) Pressure and at Higher Temperatures*; United States. Government Printing Office: Washington, DC, USA, 1995. [CrossRef]
33. Linstrom, P.J.; Mallard, W.G. NIST Chemistry WebBook, NIST Standard Reference Database Number 69. 2020. Available online: https://webbook.nist.gov/chemistry/ (accessed on 18 May 2021).
34. Stølen, S.; Grønvold, F.; Brinks, H.; Atake, T.; Mori, H. Heat capacity and thermodynamic properties of $LaFeO_3$and $LaCoO_3$fromT = 13 K toT = 1000 K. *J. Chem. Thermodyn.* **1998**, *30*, 365–377. [CrossRef]
35. Anonymous. Fire Design of Steel Structures Annex A: Thermal Data for Carbon Steel and Stainless Steel Sections. *Fire Design Steel Struct.* **2013**, 319–345. [CrossRef]
36. Abad, A.; Adánez, J.; García-Labiano, F.; de Diego, F.L.; Gayán, P.; Celaya, J. Mapping of the range of operational conditions for Cu-, Fe-, and Ni-based oxygen carriers in chemical-looping combustion. *Chem. Eng. Sci.* **2007**, *62*, 533–549. [CrossRef]
37. Xu, J.; Froment, G.F. Methane steam reforming, methanation and water-gas shift: I. Intrinsic Kinetics. *AIChE J.* **1989**, *35*, 88–96.
38. Donat, F.; Xu, Y.; Müller, C.R. Combined Partial Oxidation of Methane to Synthesis Gas and Production of Hydrogen or Carbon Monoxide in a Fluidized Bed using Lattice Oxygen. *Energy Technol.* **2020**, *8*, 1900655. [CrossRef]
39. Zaabout, A.; Cloete, S.; Amini, S. Autothermal operation of a pressurized Gas Switching Combustion with ilmenite ore. *Int. J. Greenhouse Gas Control* **2017**, *63*, 175–183. [CrossRef]
40. Ugwu, A.; Zaabout, A.; Donat, F.; van Diest, G.; Albertsen, K.; Müller, C.; Amini, S. Combined Syngas and Hydrogen Production using Gas Switching Technology. *Ind. Eng. Chem. Res.* **2021**, *60*, 3516–3531. [CrossRef]
41. Anantharaman, R.; Bolland, O.; Booth, N.; van Dorst, E.; Fernandez, E.S.; Franco, F.; Macchi, E.; Manzolini, G.; Nikolic, D.; Pfeffer, A.; et al. *Cesar Deliverable D2.4.European Best Practice Guidelines For Assessment Of CO_2 Capture Technologies*; European Commision: Brussels, Belgium, 2018. [CrossRef]
42. Khan, M.N.; Cloete, S.; Amini, S. Efficiency Improvement of Chemical Looping Combustion Combined Cycle Power Plants. *Energy Technol.* **2019**, *7*, 1900567. [CrossRef]
43. Martínez, I.; Romano, M.C.; Chiesa, P.; Grasa, G.; Murillo, R. Hydrogen production through sorption enhanced steam reforming of natural gas: Thermodynamic plant assessment. *Int. J. Hydrogen Energy* **2013**, *38*, 15180–15199. [CrossRef]
44. Gazzani, M.; Romano, M.C.; Manzolini, G. CO_2 capture in integrated steelworks by commercial-ready technologies and SEWGS process. *Int. J. Greenhouse Gas Control* **2015**, *41*, 249–267. [CrossRef]
45. Grabke, H.J.; Krajak, R.; Müller-Lorenz, E.M. Metal dusting of high temperature alloys. *Mater. Corros.* **1993**, *44*, 89–97. [CrossRef]
46. Zhang, X.; Keramati, H.; Arie, M.; Singer, F.; Tiwari, R.; Shooshtari, A.; Ohadi, M. Recent developments in high temperature heat exchangers: A review. *Front. Heat Mass Transf.* **2018**, *11*. [CrossRef]
47. Jonsson, M.; Bolland, O.; Bücker, D.; Rost, M. Gas Turbine Cooling Model for Evaluation of Novel Cycles. Available online: https://www.researchgate.net/profile/Olav-Bolland/publication/237502557_Gas_turbine_cooling_model_for_evaluation_of_novel_cycles/links/56794cc208ae6041cb49f38a/Gas-turbine-cooling-model-for-evaluation-of-novel-cycles.pdf (accessed on 20 May 2021).
48. Horlock, J.H. *Advanced Gas Turbine Cycles*; Elsevier: Amsterdam, The Netherlands, 2003.
49. Sanjay, O.S.; Prasad, B.N. Influence of different means of turbine blade cooling on the thermodynamic performance of combined cycle. *Appl.Therm. Eng.* **2008**, *28*, 2315–2326. [CrossRef]
50. Chiesa, P.; Macchi, E. A Thermodynamic Analysis of Different Options to Break 60% Electric Efficiency in Combined Cycle Power Plants. *J. Eng. Gas Turbines Power Trans. ASME* **2004**, *126*, 770–785. [CrossRef]
51. Gülen, S.C. *Gas Turbines for Electric Power Generation*; Cambridge University Press: Cambridge, UK, 2019.
52. Inoue, K.; Miyamoto, K.; Domen, S.; Tamura, I.; Kawakami, T.; Tanimura, S. Development of hydrogen and natural gas co-firing gas turbine. *Mitsubishi Heavy Ind. Tech. Rev.* **2018**, *55*, 1.
53. Cloete, S.; Romano, M.C.; Chiesa, P.; Lozza, G.; Amini, S. Integration of a Gas Switching Combustion (GSC) system in integrated gasification combined cycles. *Int. J. Greenhouse Gas Control* **2015**, *42*, 340–356. [CrossRef]

54. del Pozo, C.A.; Cloete, S.; Chiesa, P.; Álvaro, Á.J.; Amini, S. Integration of gas switching combustion and membrane reactors for exceeding 50% efficiency in flexible IGCC plants with near-zero CO_2 emissions. *Energy Convers. Manag. X* **2020**, *7*, 100050.
55. Siemens-Energy. Available online: https://www.siemens-energy.com/global/en/offerings/power-generation/gas-turbines/sgt-800.html (accessed on 18 May 2021).
56. Campanari, S.; Mastropasqua, L.; Gazzani, M.; Chiesa, P.; Romano, M.C. Predicting the ultimate potential of natural gas SOFC power cycles with CO_2 capture—Part A: Methodology and reference cases. *J. Power Sources* **2016**, *324*, 598–614. [CrossRef]
57. Pipitone, G.; Bolland, O. Power generation with CO_2 capture: Technology for CO_2 purification. *Int. J. Greenhouse Gas Control* **2009**, *3*, 528–534. [CrossRef]